Working Report 2011-16

Semi-Integration of Overcoring Stress Data and Review of Rock Stress Data at the Olkiluoto Site

Daniel Ask

June 2011

POSIVA OY
Olkiluoto
FI-27160 EURAJOKI, FINLAND
Tel +358-2-8372 31
Fax +358-2-8372 3709

Working Report 2011-16

Semi-Integration of Overcoring Stress Data and Review of Rock Stress Data at the Olkiluoto Site

Daniel Ask

Vattenfall Power Consultant AB

June 2011

SEMI-INTEGRATION OF OVERCORING STRESS DATA AND REVIEW OF ROCK STRESS DATA AT THE OLKILUOTO SITE

ABSTRACT

This project involves a semi-integration of collected rock stress data at Olkiluoto. The data included in the study involves overcoring and hydraulic fracturing data reported in the 2006 Site Report, supplemented with the additional data gathered since then, measurements for the power plant construction, and measurements in ONKALO. Despite the extensive data, and although the data display a fair correspondence with respect to stress magnitudes between methods, a few discrepancies between methods exist. The discrepancies primarily concern the orientation of the horizontal stresses and the magnitude of maximum horizontal stress.

The objective of the study is help answer the remaining discrepancies in the collected data using a semi-integration approach on the overcoring data, i.e. a simplified application of the Integrated Stress Determination Method.

The semi-integration involves two steps: (i) a brief re-evaluation of data; and (ii) forced overcoring stress calculations based on constraints derived from the other stress measurement techniques. The overall intension was to force overcoring data, which is the method displaying the largest scatter in results at the Olkiluoto site, to be consistent with a number of constraints that were derived from other stress measurement techniques. This exercise would outline the most probable constraints and in the extension, help identifying a stress model for the site.

Regrettably, the results of the semi-integration were not completely satisfactory. The most important factor of this outcome is believed to be the failure to reduce the initial scatter through a re-evaluation. The remaining scatter after re-evaluation is judged too large to represent solely *in situ* stress variation; hence, measurement related errors are likely still present in the re-evaluated data set. A more in-depth analysis may to some extent decrease the scatter in data, but perhaps more effectively, develop a tool that simultaneously can derive the stress field from all stress measurement techniques.

The variability in results is visualized by the low consistency of overcoring strains with the various constraints, although they clearly may represent also improperly defined constraints but may also reflect a reduced data quality or limitations of the acceptance criteria and algorithm.

What can be concluded is that one principal stress is indeed vertical (or near vertical) and closely resembles the theoretical weight of the overburden. The results of constraining also horizontal stress orientations and magnitudes are though much less clear. Most likely, σ_H is directed NW-SW, i.e. a quite imprecise result.

The report also involved analysis of observed core discing. The results of this study show that dominating disc type at the Olkiluoto site is the incomplete disc (52 % of all observations) and the dominating host rock pegmatitic granite (PGR; 49 % of all

observations). Discing events with other disc shapes and in other rock types are significantly less frequent.

The discing events could not be correlated with existing and larger deformation zones, although discing events may possibly be correlated to zone OL-BFZ002. Note that the analysis has only been made with respect to the major deformation zones, which does not preclude that discing events may be correlated to smaller scale zones.

Horizontal stress magnitudes for the dominating rock types were determined using nomograms and it was found that the result for the pegmatitic granite and the diatexitic gneiss fit well with the results from the semi-inversion, whereas the results for both mafic and veined gneisses seem to overestimate the horizontal stress magnitudes.

In the final chapter, an attempt to describe the prevailing general stress field at the Olkiluoto site is presented. The suggested model is based on multiple stress sources but without placing weight to the various methods.

Keywords: Olkiluoto, nuclear waste disposal, semi-integration, stress measurements, overcoring, hydraulic fracturing, hydraulic tests on pre-existing fractures, convergence measurements, acoustic emission, core discing

KALLION JÄNNITYSTILAMITTAUSTULOSTEN KOKONAISARVIOINTI OLKILUODON TUTKIMUSALUEELLA

TIIVISTELMÄ

Tämä raportti käsittelee Olkiluodossa suoritettujen kallion jännitystilamittaustulosten kokonaisvaltaista arviointia. Tutkimusaineisto käsittää Olkiluodon Paikkaraportissa 2006 esitetyt irtikairaustulokset ja hydraulisen murtamisen mittaustulokset sekä sen jälkeen tehdyt eri jännitystilamittaukset alueella. Huolimatta laajasta mittausaineistosta, ja vaikka tulokset eri menetelmillä ovat melko yhteneviä jännitysten suuruuksien osalta, niin joitakin eroja eri menetelmien kesken esiintyy. Erot liittyvät lähinnä vaakajännitysten suuntiin ja suurimman vaakajännityksen suuruuteen.

Tämän työn tavoitteena oli yrittää löytää vastauksia tulosten eroavaisuuksiin käyttämällä ns. irtikairaustulosten semi-integraatio analyysiä. Analyysi käsittää kaksi vaihetta: (i) lyhyt tulosten uudelleenarviointi ja (ii) kallion jännitysten laskeminen käyttämällä muista mittausmenetelmistä saatuja reunaehtoja. Tavoitteena oli pakottaa irtikairaustulokset, joissa oli todettu runsaasti hajontaa, sopimaan muiden mittausmenetelmien antamiin reunaehtoihin. Työn tarkoituksena oli löytää todennäköisimmät rajoitukset/reunaehdot ja siten paremmin tunnistaa tutkimusalueen jännitystilamalli.

Tulokset suoritetusta analyysistä eivät kuitenkaan valitettavasti olleet täysin tyydyttäviä. Tulosten uudelleenarvioimisessa tulosten hajontaa ei pystytty juurikaan pienentämään. Tulosten hajonta jäi liian suureksi pelkästään jännitystilan vaihtelusta johtuvaksi eli erilaiset mittausvirheet ovat todennäköisesti edelleen liian voimakkaina mukana tuloksissa. Syvällisempi analyysi voisi ehkä hajontaa pienentää, mutta tehokkaampi tapa olisi ehkä työkalun kehittäminen, joka samanaikaisesti huomioisi kaikki eri menetelmien mittaustulokset.

Eri reunaehtoja käytettäessä irtikairausmittausten muodonmuutostuloksia ei saatu yhteneviksi. Tämä saattoi johtua siitä, että reunaehdot eivät olleet riittävän täsmällisesti määritettyjä tai mittausten laatu oli huonoa tai hyväksyttävyyskriteerien rajoituksista.

Tuloksista voitiin kuitenkin varmuudella todeta, että yksi pääjännityksistä on pysty tai lähes pysty ja vastaa kallion omasta painosta johtuvaa jännitystä. Vaakajännitysten suuntien ja suuruuksien määrittäminen oli selvästi vaikeampaa. Suurimman vaakajännityksen suunta luode-kaakko on suhteellisen epäluotettava tulos.

Raportissa on analysoitu myös kairasydännäytteiden viipaloitumista ns. core discing-ilmiötä. Yleisin viipaloitumistyyppi on epätäydellinen viipaloituminen (52 % kaikista havainnoista) ja vallitsevin kivilajiympäristö on pegmatiitti-graniitti (49 % kaikista havainnoista). Muut viipaloitumistyypit ja viipaloituminen muissa kivilajeissa on selvästi harvinaisempaa.

Kairasydännäytteiden viipaloitumista ei voitu liittää olemassa oleviin ja suurimpiin deformaatiovyöhykkeisiin, vaikkakin niitä saattaa liittyä vyöhykkeeseen OL-BFZ002. On myös huomattava, että vaikka analyysi tehtiin liittyen suurimpiin deformaatio-

vyöhykkeisiin, niin se ei poissulje sitä, että viipaloitumista voi liittyä pienemmän mittakaavan vyöhykkeisiin.

Vaakajännityksiä tarkasteltiin myös eri kivilajiympäristöissä ja voitiin todeta, että pegmatiittisen-graniitin ja diatekstiittisen gneissin tulokset olivat yhteneviä semi-inversio tuloksen kanssa, kun taas sekä maafisen gneissin että suonigneissin tulokset pyrkivät yliarvioimaan vaakajännitysten suuruuksia.

Raportin lopussa on pyritty arvioimaan Olkiluodon vallitsevaa jännitystilaa. Esitetty jännitystilamalli perustuu useisiin jännitystilamittauslähteisiin, mutta näiden keskinäistä painotusta ei ole tehty.

Avainsanat: Olkiluoto, ydinjätteiden loppusijoitus, semi-integraatio analyysi, jännitys-tilamittaukset, irtikairausmenetelmä, hydraulinen murtaminen, konvergenssimittaukset, akustinen emissio, kairasydännäytteiden viipaloituminen

TABLE OF CONTENTS

LIST OF SYMBOLS

σ_H = major horizontal stress

σ_h = minor horizontal stress

σ_v = vertical stress

α_v = vertical stress gradient

σ_T = tensile strength

P_b = breakdown pressure

P_p = pore pressure

ε_i = strain gauge number i

ν = Poisson's ratio

1 INTRODUCTION

This report describes a semi-integration study of collected rock stress data at Olkiluoto commissioned by Posiva Oy and conducted by Vattenfall Power Consultant AB. In the study, overcoring data are examined for consistency with respect to data from other measurement methods. In addition, a general summary of all collected stress data at the Olkiluoto site is presented (Chapter 5).

The Olkiluoto site is located approximately 25 km north of Rauma on the west coast of Finland (Figure 1-1). In December 2000, the Finnish Government made a decision-in-principle that "it is in agreement with the society total interest to construct a final repository in Olkiluoto" (Government Decision December 21, 2000, ratified by Parliament on May 18, 2001). In the decision in principle, it is also stated that further investigations will be needed. The continued investigation of the Olkiluoto site will focus on the construction and operation of an underground rock characterization facility called the ONKALO.

In order to support rock engineering design, the rock mechanics analyses and the Prediction-Outcome work for the ONKALO, a better understanding of the in situ stress field and especially the stress tensor is required. The access ramp of the ONKALO facility is now being excavated and, in March 2008, it has reached ~2400 m, which is equivalent to the depth of about 240 m – please update this.

The data included in the study involves those reported in the 2006 Site Report (Klasson and Leijon 1990; Ljunggren and Klasson 1996; Sjöberg 2003; Lehtonen 2005), supplemented with the additional data gathered since then (Fecker 2007; Lehtonen 2005, 2008; Hakala 2008; Ask et al. 2010a, b), measurements for the power plant construction (SMOY, 2006), shaft response and shaft strain measurements in ONKALO in 2007 and 2008 (Hakala 2008), overcoring measurement campaign in ONKALO in 2008 (Berg 2008), and the latest hydraulic stress measurement campaign in 2008 (Ask et al. 2010a, b), and measurements using long strain gauges (LSG; Hakala 2010a) and Linear Variable Differential Transducers (LVDTs; Hakala 2010b). The data included in this report are summarized in Table 1-1.

The geological conditions at the measurement site in ONKALO are characterized by crystalline bedrock, dominated by migmatic and foliated mica gneiss. Massive, coarse-grained granites and pegmatites also occur in the area. The general foliation is estimated to be about 160/40°. Based on observations from the access tunnel, horizontal or sub-horizontal, south-east-dipping fractures dominate. Another fracture set strikes approximately north south and dips steeply to the east or west. Additionally there are sub vertical east-west striking fractures.

A specific chapter is devoted to observed core discing in multiple drillholes (Chapter 4). The purpose of this chapter is to summarize all core discing data and attempt to distinguish if core discing is more prone to appear in specific rock types or are concentrated to specific geological features such as fracture zones. In addition, attempts are made to determine stress magnitudes using nomograms developed by Hakala (1999a, 1999b). Note that the core dicing data is a free-standing data set that is not considered in the semi-integration analysis.

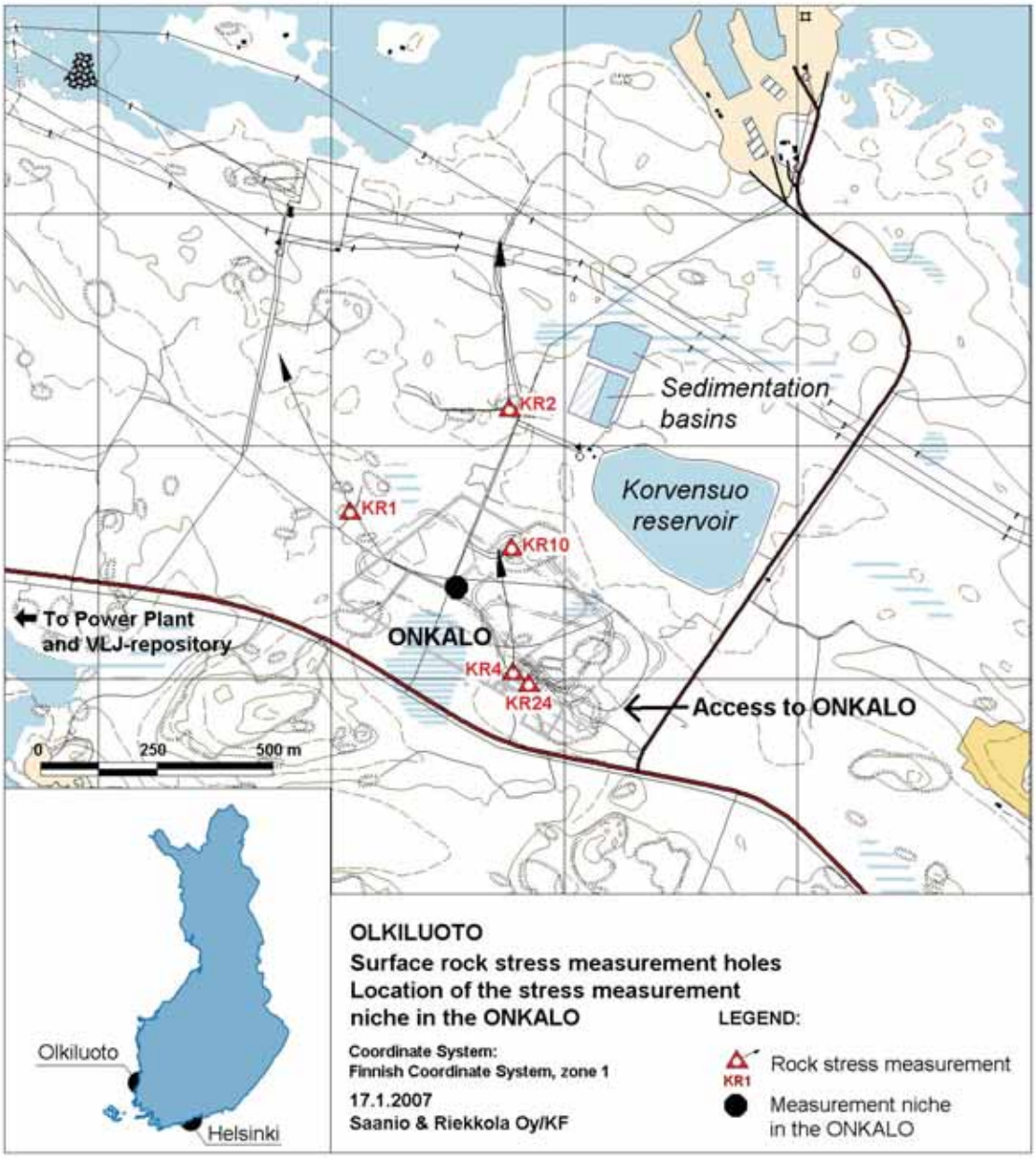

Figure 1-1. *Map of the Olkiluoto site, showing the location of ONKALO where the stress measurements were conducted. Should be a new figure where OL-KR40 is included.*

Table 1-1. *Rock stress data considered in this report.*

Drillhole	Measurement technique	Depth [mvd]	Inclination (from horizontal)
OL-KR1[1]	HF	448-809	70-64
OL-KR2[2]	HF	296-799	72-66
OL-KR4[2]	HF	274-710	76-70
OL-KR10[2]	HF	337-520	85-83
OL-KR40[3]	HF/HTPF	122-800	70-58
ONK-PP125[3]	SF/HF	207-253	90
OL-KR10[2]	OC	301-613	90
OL-KR24[4]	OC	310-390	90
ONK-PP74[5]	OC	130	44.9
ONK-PP75[5]	OC	132	44.5
ONK-PP77[5]	OC	119	-4.7
JMT-1[6]	OC	18	-2
ONK-PP169[7]	OC	237	-29.8
ONK-PP170[7]	OC	224	10.5
Ventilation/Personal shafts[8,9,10]	CM	155-280	90
	LSG	155-280	90
	LVDT	155-280	90
OL-KR14[11]	AE	80-500	
OL-KR28[12]	AE	344	
OL-KR29[12]	AE	344-657	

Key: HF denotes Hydraulic Fracturing, HTPF denotes Hydraulic Tests on Pre-existing Fractures, SF denotes Sleeve Fracturing, OC denotes OverCoring, CM denotes Convergence Measurements, LSG denotes Long Strain Gauges, LVDT denote Linear Variable Differential Transducer, AE denotes Acoustic Emission.

1 Klasson and Leijon, 1990
2 Ljunggren and Klasson, 1996
3 Ask et al., 2010a; b
4 Sjöberg, 2003
5 Fecker, 2007
6 SMOY, 2006
7 Berg, 2008
8 Hakala, 2008
9 Hakala, 2010a – LSG report
10 Hakala, 2010b – LVDT report
11 Lehtonen, 2005
12 Lehtonen, 2008

2 DATA VERIFICATION PRIOR TO SEMI-INTEGRATION

2.1 General

The basic premise of the semi-integration was to investigate how many of the collected overcoring strains that are consistent with results from other measurement techniques. Prior to this investigation, all the data were first re-evaluated, aiming at identifying and removing obviously doubtful data from each measurement technique. This, re-evaluated set of data, are denoted unambiguous. In the next phase, a number of constraints are derived based on density measurements on cores, results from hydraulic fracturing data, and finally, convergence measurements. These constrains are subsequently used in forced overcoring stress calculations, i.e. the overcoring strains are forced to be consistent with each of the constraints (Chapter 3).

The re-evaluation of the previously collected data generally follow the directions outlined in the Suggested Methods by International Society of Rock Mechanics (ISRM), i.e. the papers by Haimson and Cornet (2003) for hydraulic data and Sjöberg et al. (2003) for overcoring data. The re-evaluation focuses on identifying measurement-related uncertainties that may reduce the reliability or disqualify the data. Note that, no attempts are made to find the source of the problem. Instead, doubtful data are simply discarded. However, in Chapter 2.10, possible correlation between overcoring results and existing fractures and foliation is made.

Results from acoustic emission were given from Posiva and was not re-evaluated.

2.2 Overcoring rock stress data

The analysis of the overcoring data primarily involves consideration to validity of the CHILE-condition, i.e. continuous, homogeneous, isotropic, and linear-elastic behavior during glue hardening, overcoring, and biaxial testing. Data that indicate deviations from these pre-requisites are discarded. This implies that, in some cases, measurement points may not contain sufficient information to solve the full stress tensor in the point in question.

As a result of that some tests may not contain sufficient information to solve the full stress tensor, the overcoring data were divided into two scales: (i) the single test scale; and (ii) the measurement level scale (Table 2-1). At the single test scale, ambiguous strain data are still used, whereas they are removed at the measurement level scale. In case elastic parameters are missing, results from adjacent tests are used during calculation (valid for both scales).

2.2.1 Results of re-evaluation

Table 2-1 present the measurement levels, which drillholes that the data originates from, the type of overcoring cell employed, the number of overcoring and biaxial strains available at each level, and finally, the number overcoring and biaxial strains that were deemed unambiguous and subsequently used in forced overcoring stress calculations (Chapter 3).

The results indicate that the success rate for CSIRO HI was unusually low and only about 23 % of both overcoring and biaxial strains data are useful. The results from the Borre Probe (Figure 2-1) is considerably better (82 and 66 % of the overcoring and biaxial strains, respectively, data are useful) although a significant amount of strains also for this cell were found ambiguous.

Table 2-1. *Measurement levels for overcoring rock stress data.*

Level	Depth [mvd]	Involved drillholes	Cell (no. strain gauges)	Total no. strains[1,2]	No. unambiguous strains[3]; (%/%)
1	20	JMT-1	CSIRO HI (12)	36/21	12/7 (33%/33%)
2	125	ONK-PP74, ONK-PP75, ONK-PP77	CSIRO HI (9)	72/40	13/7 (18%/18%)
3	240	ONK-PP170	Borre Probe (9)	36/24	26/17 (72%/71%)
4	320	OL-KR10, OL-KR24	Borre Probe (9)	54/36	46/26 (85%/72%)
5	390	OL-KR24	Borre Probe (9)	18/12	17/6 (94%/50%)
6	450	OL-KR10	Borre Probe (9)	54/36	54/24 (100%/67%)
7	605	OL-KR10	Borre Probe (9)	54/36	34/22 (63%/61%)

Key: [1]Overcoring strains versus biaxial strains; [2]Total number of strains reflects reported successful data and not overcoring attempts; [3]No of unambiguous overcoring strains versus unambiguous biaxial strains.

Figure 2-1. *Photo showing the Borre Probe, employed in drillholes ONK-PP170, OL-KR10, and OL-KR24.*

2.3 Density measurements on cores

Results from density measurements from cores were provided by Posiva and were not re-evaluated. The results yield that (reference)

$$\alpha_{v,theory} = 0.0265 \text{ MPa/m} \quad (2.1)$$

2.4 Hydraulic fracturing data

2.4.1 Previously collected data

The re-evaluation of the previously collected hydraulic stress data (Klasson and Leijon 1990; Ljunggren and Klasson 1996) focuses entirely on the hydraulic fracturing data (HF). Hence, no attempts are made to use test where pre-existing fractures have been stimulated, although in some drillholes, they are numerous.

The analysis of HF data focuses on the orientation of the induced fractures (i.e. imprints with axial fractures in the direction of minimum horizontal stress) and the magnitude of maximum horizontal stress (σ_H) from pressure versus time plots. For orientations, all imprints are re-evaluated with respect to both orientation device (single-shot magnetic compass) and fracture inclination. In case multiple fractures appear, only the orientation data are used, whereas the pressure data are regarded ambiguous and thus discarded.

For the σ_H-magnitude, a key features to be verified is the appearance of the breakdown pressure. The breakdown pressure is defined as the maximum pressure observed during the fracturing cycle. For a correct analysis of the σ_H-magnitude, the breakdown must be distinct. If it is non-linear, this may be an indication of progressive fracture extension with correlative fluid penetration, long before breakdown is reached. Indeed, if the stress at the drillhole wall is tensile, but lower than the tensile strength, the fluid percolation will not be axisymmetric but rather a preferential percolation within the zone of tensile stress so that the classical HF is simply not valid, as it will underestimate the breakdown pressure. Cornet (1989) demonstrated this at the Moodus site in Conneticut. All tests with non-linear pressurization rate prior to fracture initiation were thus discarded. The σ_H-magnitude is evaluated using (Amadei and Stephansson 1997):

$$\sigma_H = 3*\sigma_h - P_b + \sigma_T - a*P_p \quad (2.2)$$

where σ_h and σ_H are the minimum and maximum horizontal stresses, P_b is the breakdown pressure, σ_T is the tensile strength, P_p is pore pressure, and a is an unknown constant between 0 and 1. The pore pressure is unknown because the permeability, in the extension zone close to the drillhole before failure occurs, is stress dependent. The extreme values occur for (1) a = 0, P_p value arbitrary; and (2) a = 1 and $P_p = P_b$, giving the maximum and minimum magnitudes for σ_H, respectively.

Consequently, we do not support application of the modified hydraulic fracturing equation that is based on re-opening pressure (Bredehoeft et al. 1976). In the scientific world, because it is assumed that the re-opening is solely a result of overcoming the

hoop stress around the drillhole, the assumption that the stress field remains the same in the fractured and unfractured rock has been questioned because the hoop stresses for the two cases cannot be the same. This was studied first by Ratigan (1992), and later by Rutqvist et al. (2000), who found that the estimate of maximum horizontal stress should be based on breakdown pressure and tensile strength. A related study by Ito et al. (1999), showed that even if the results by Ratigan (1992) and Rutqvist et al. (2000) would be wrong, i.e. employment of re-opening is theoretically valid, the re-opening pressure cannot, with most available equipments, be properly identified due to the compliance of the testing system. An identification better than 10 % from the true value would require a system compliance of $5 \cdot 10^{-7}$ m^3/MPa, which is several orders of magnitude less than that of most existing systems. In addition, the re-opening pressure is known to be flow-rate dependent and there is no guarantee that the chosen flow rate is high enough to prevent fluid penetration prior to re-opening. Finally, it is very difficult to verify that the pore pressure has not returned to its original value prior to initiation of pressurization.

The magnitude of minimum horizontal stress (σ_h), i.e. the shut-in pressure on pressure versus time plots, was originally interpreted using the graphical tangent intersection method of Enever and Chopra (1989). Thus, the ISRM suggested methods (Haimson and Cornet, 2003) *dt/dP* versus *P*-method of Hayashi and Haimson (1991), the Muscat method of Aamodt and Kuriyagawa (1981), or the *dP/dt* versus *P*-method of Lee and Haimson (1989) were not employed. Because the applied tangent intersection method is known to underestimate the normal stress, they were re-evaluated using the inflection point method (Gronseth and Kry 1981; which is known to yield un overestimate of σ_h) and Muskat method (Aamodt and Kuriyagawa 1981; which is known to yield un underestimate of σ_h). However, because the data is not digital, these methods were applied with visual inspection. This action results in normal stresses that are about 1.0 to 1.5 MPa larger than the original interpretation (thus increasing the σ_H-magnitude with 3-4.5 MPa).

2.4.2 Results of re-evaluation of previously collected data

Regrettably, only raw data from drillhole OL-KR1 were recovered at the time of this report. Overall, the re-evaluation basically confirmed previous interpretation (Figure 2-2) and the data clearly indicate that one principal stress is vertical. Moreover, because drillhole OL-KR1 is slightly inclined with respect to the vertical direction (20-26^o), a number of tests (4) show en echelon fractures, which is to be expected when the drillhole is inclined more than 15-20 degrees from a principal stress direction. The results of the re-evaluation is as follows (solution at 400 mvd and assumed valid between 200-850 mvd):

$\sigma_h = 10.7+0.0321*(z-400)$ MPa; (2.3)
$\sigma_H = 16.6+0.0712*(z-400)$ MPa; (2.4)
Orientation of $\sigma_H = 92 \pm 18^o$N. (2.5)

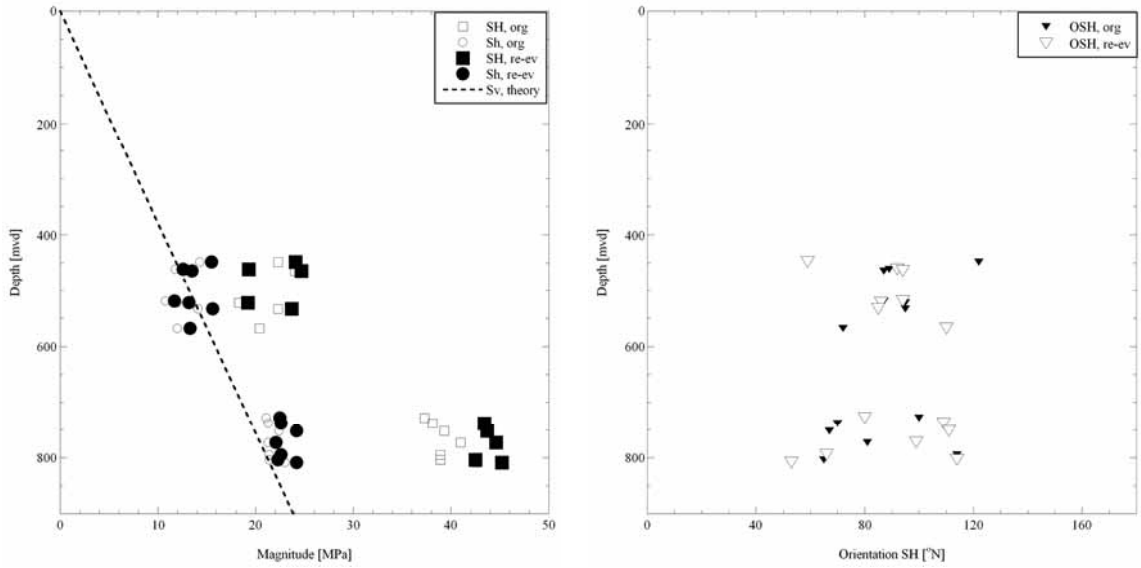

Figure 2-2. *Original and re-evaluated results from hydraulic fracturing in drillhole OL-KR1; horizontal stress magnitudes (left) and orientations (right).*

2.4.3 Recently collected data and their results

Stress measurement data were collected during year 2008 in drillholes OL-KR40 and ONK-PP125 (Ask et al. 2010a; b; Figure 2-3). These data set and the interpretation schemes followed the directions outlined by ISRM (Haimson and Cornet 2003) and were not re-evaluated.

As drillhole OL-KR40 is significantly inclined with respect to the vertical direction (about 70^{o} at the drillhole collar and about 58^{o} at 1000 mbl), the primary testing procedure involved stimulation of pre-existing fractures, i.e. using the HTPF technique. Because axial fractures cannot be produced that simultaneously determines 4 of the six unknown tensor components, the resolution of the stress calculation in drillhole OL-KR40 was not optimal. Of this reason, a specially developed code for investigation of failure criterion was employed to verify the obtained solution and to help constrain the magnitude of maximum horizontal stress.

For drillhole ONK-PP125, which is nearly perfectly vertical, unanticipated results were also obtained. In this drillhole, despite the application of both sleeve fracturing and hydraulic fracturing technique, axial fractures could not be produced. In addition, the small number of tests available in the short drillhole rendered the conventional analysis methodology ambiguous. Also for this drillhole, the special failure code was employed, giving significantly improved information.

The results from stress calculation and verification with the failure criterion code are presented in Figure 2-4. Interestingly, the recently and previously collected data show very similar orientations and horizontal stress gradients versus depths, but the stress magnitudes are higher in the recently collected data set compared with the previously collected:

σ_h = 16.6+0.0225*(z-400) MPa; (2.6)
σ_H = 22.6+0.0225*(z-400) MPa; (2.7)
Orientation of σ_H = 80°N. (2.8)

This solution is valid strictly between 150-500 mvd, but it will in this report be assumed valid down to the depths of the deepest overcoring test (about 600 mvd).

Figure 2-3. *Photo from the hydraulic stress measurements in drillhole OL-KR40, 2008.*

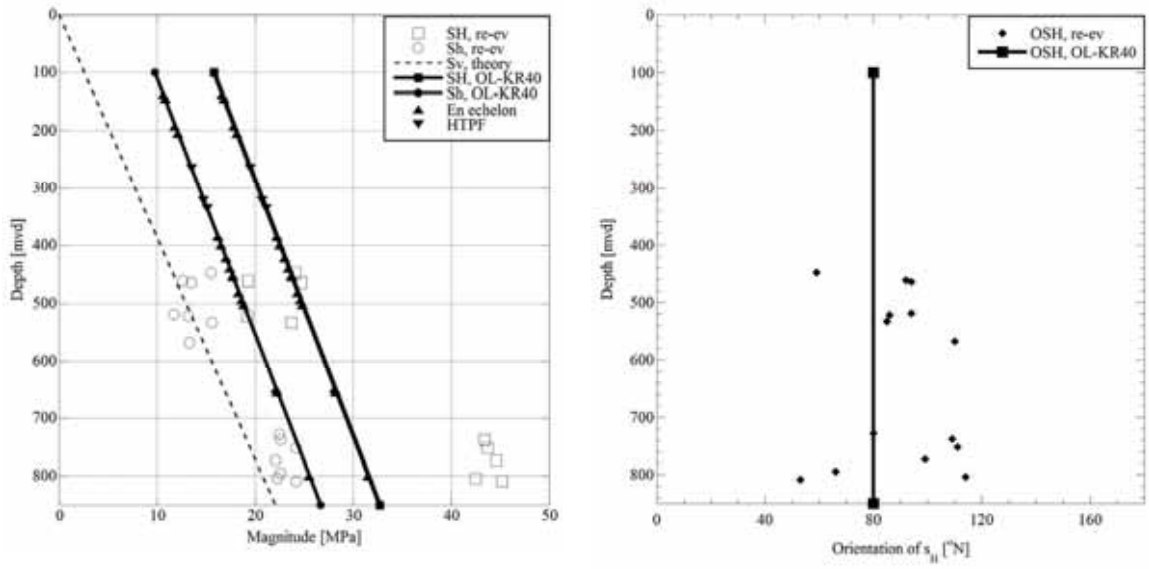

Figure 2-4. *Previously collected and re-evaluated data shown together with recently collected data; horizontal stress magnitudes (left) and orientations (right).*

2.5 Convergence data

Convergence measurements (CM) have been undertaken at the 180 and 280 m levels in the shafts at ONKALO (KU1 to KU3). Apart from shaft KU3, the repeatability f the measurements are very poor. For shafts KU1 and KU2, both measurements levels, only 14 % of the measurements are repeatable when using 0.03 mm as cut off. Hence, nothing useful can be derived from those tests.

For shaft KU3, 93 % are repeatable and the results indicate that maximum horizontal stress is directed E-W at the 180 m level and NE-SW at the 280 m level, respectively. However, the upper test is judged unrealistic as the test suggests increasing in the N-S direction (unchanged diameter in the E-W direction). Thus, only one out of six tests is considered useful (Figure 2-5). The state of stress for this test (2D solution) suggests that (Figure 2-6):

$\sigma_h = 2.7$ MPa; (2.9)
$\sigma_H = 6.1$ MPa; (2.10)
Orientation of $\sigma_H = 156^oN$. (2.11)

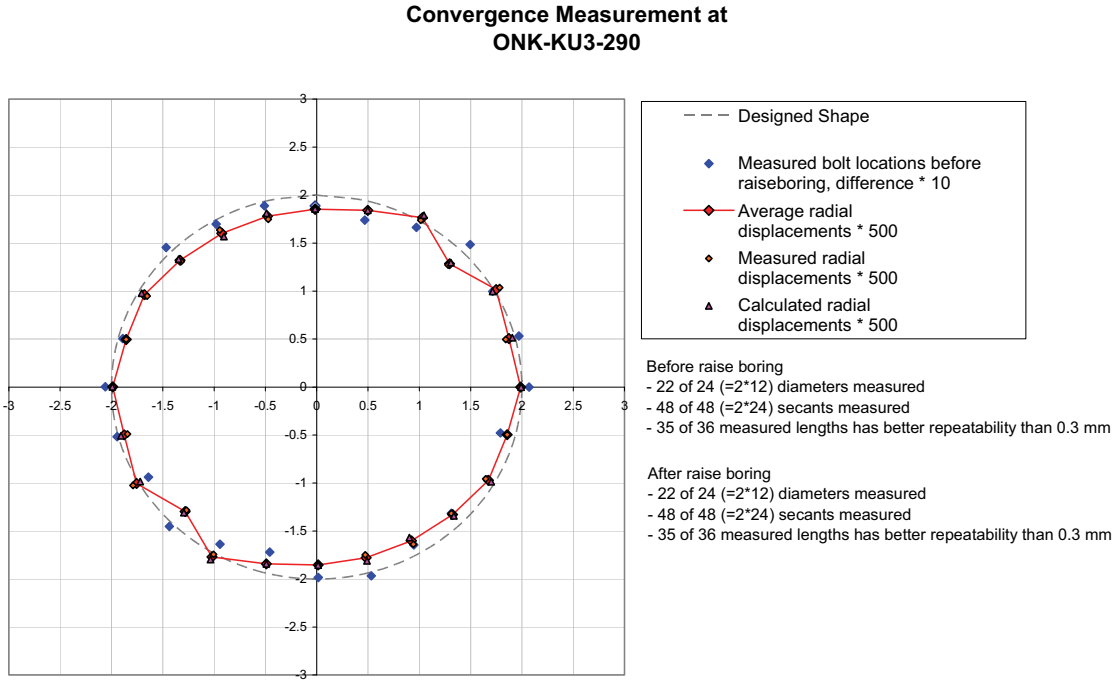

Figure 2-5. *Previously collected and re-evaluated data shown together with recently collected data; horizontal stress magnitudes (left) and orientations (right).*

2.6 Acoustic emission

Results used from acoustic emission (AE) in drillholes OL-KR14, OL-KR28, and OL-KR29 involved only the most reliable data from Lehtonen (2005) and Lehtonen (2008). Yet, it should be pointed out that the internal error within the AE data is significant and the method must be regarded as crude. The results are presented in Figure 2-6 together with data from convergence measurements at 280 mvd. The combined result from AE and CM is quite inconclusive. Yet, following equations were derived and used in the semi-integration phase.

$\sigma_h = 7.8+0.0045*(z-400)$ MPa; (2.12)
$\sigma_H = 14.8+0.0180*(z-400)$ MPa; (2.13)
Orientation of $\sigma_H = 30^oN$. (2.14)

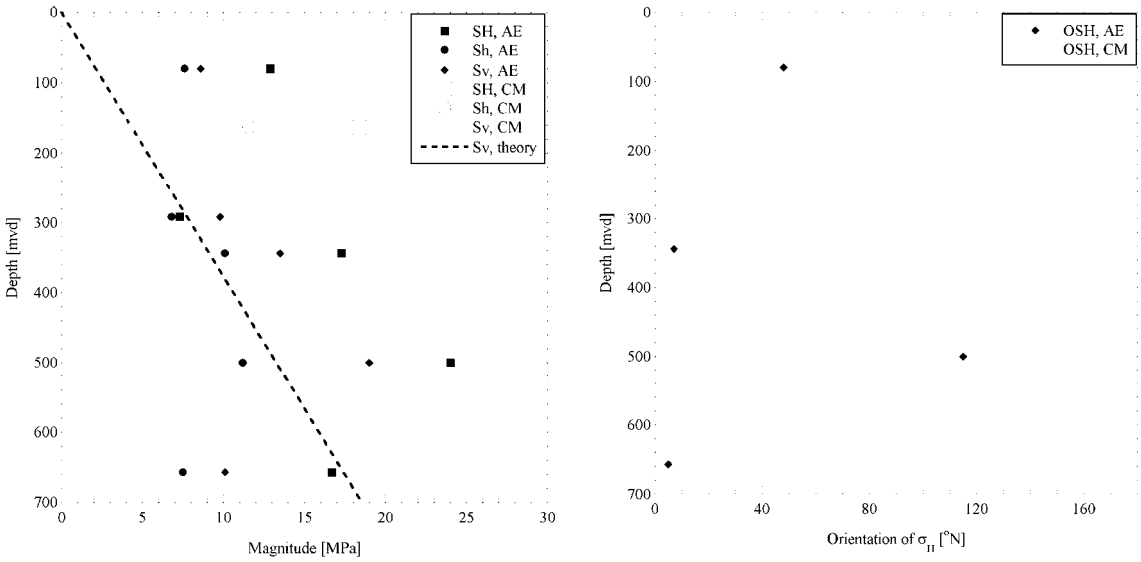

Figure 2-6. *Results from acoustic emission (Lehtonen, 2005, 2008) and convergence measurements (Hakala, 2008); horizontal stress magnitudes (left) and orientations (right).*

2.7 Long strain gauges

As an attempt to reduce the considerable scatter observed in the results using conventional overcoring at the Olkiluoto site, tests were made using long strain gauges (LSD; 50 mm long; Hakala, 2010a). The measurements were conducted in the large size raise boring shafts, implying that the tests are essentially a very large overcoring test. Similar to the CSIR-cells, a number of strain rosettes with three strain gauges were used with a set-up that allow determination of the full stress tensor (Figure 2-7). The gauges were subsequently overcored using 120/127 (OD_{core} = 120 mm) overcoring drill bit. Finally, the core was tested in a biaxial cell to derive elastic parameters.

The data were evaluated using the same methodology as for overcoring tests and is therefore not repeated here. The results are displayed in Figure 2-9 and represent the 2D solution without temperature correction.

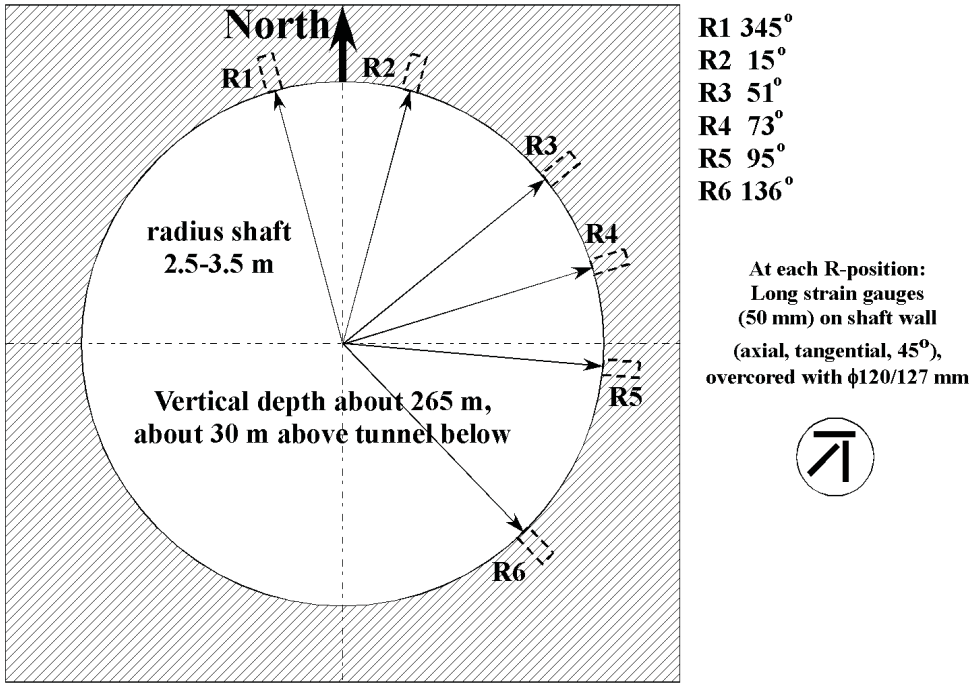

Figure 2-7. *Configuration of the test in the outlet air shaft (265 mvd). Rosettes 1 to 6 are oriented –15 °, 15 °, 51 °, 73 °, 95 °, and 136° with respect to North. The strain gauges are oriented axially, horizontally, and 45°-inclined from the axial direction.*

2.8 LVDT measurements

The measurements using LVDTs (Hakala 2010b) have been conducted in the outlet air shaft at the 265 level (Figure 2-8), EDZ niche at the 345 level, and in the ramp chainage, sections 3662 (349 mvd), 4020 (348 mvd), and 4186 (399 mvd). In principle, testing is similar to the cell developed by the US Bureau of Mines, denominated USBM gage (e.g. Merril 1967; Hooker et al. 1974). As for the USBM gage, diametrical deformations are measured, but the dimensions of the ONKALO tests are significantly larger: the cell is mounted in a ϕ127 mm drillhole and is subsequently overcored using ϕ200 mm drill bit. The core was as a result of its size, not tested in a biaxial cell to derive elastic parameters. Instead the solid core, i.e. “the pilot drillhole core”, was tested in biaxial test chamber.

Given the similarities of the LVDT tests with conventional overcoring and the USBM cell, the re-evaluation generally follows the directions outlined in the latest Suggested Methods by International Society of Rock Mechanics (ISRM; Sjöberg et al., 2003), but also the issue of 1987, describing the USBM gage (Kim and Franklin, 1987), was consulted. The re-evaluation focused on identifying measurement-related uncertainties that may reduce the reliability or disqualify the data. Note that, no attempts are made to find the source of the problem. The results, together with long strain gauges, suggest that stresses in the interval 150-400 mvd are as follows:

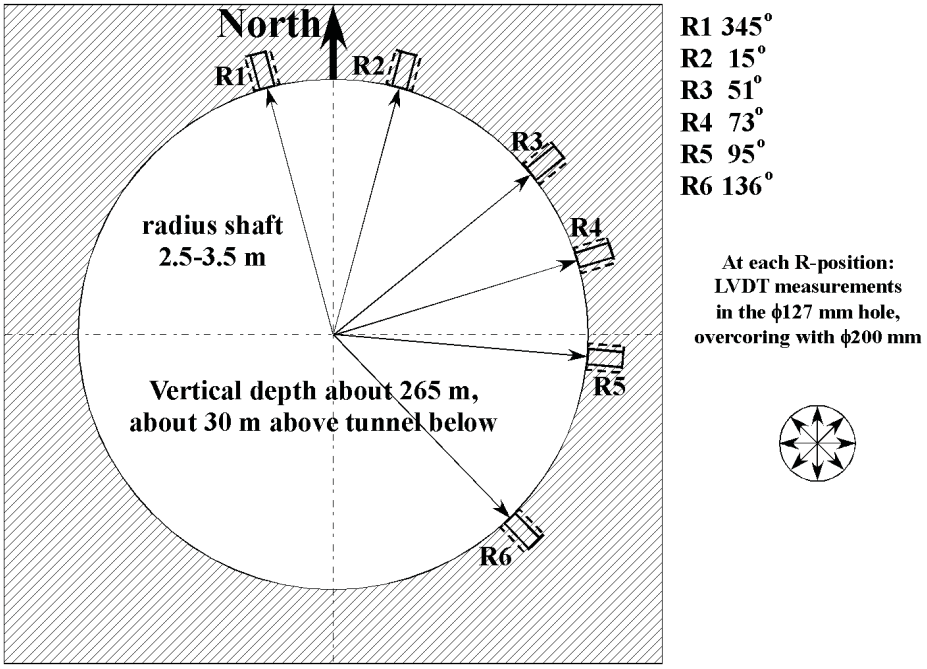

Figure 2-8. *Configuration of the test in the outlet air shaft at about 265 mvd. Rosettes 1 to 6 are oriented –15°, 15°, 51°, 73°, 95°, and 136° with respect to North.*

σ_h = 14.2-0.0139*(z-400) MPa; (2.15)
σ_H = 25.5+0.0153*(z-400) MPa; (2.16)
Orientation of σ_H = 106°N. (2.17)
σ_v = 14.1-0.0312*(z-400) MPa (2.18)

It should be noted that the LVDT tests at 156 and 399 mvd constrains the gradients of σ_h and σ_v completely (Figure 2-9). With those tests excluded, the data suggest that both σ_h and σ_v are basically constant in the interval 150-400 mvd. Thus, the equations used for defining constraints are:

σ_h = 14.2 MPa; (2.19)
σ_H = 25.5+0.0153*(z-400) MPa; (2.20)
Orientation of σ_H = 106°N. (2.21)
σ_v = 14.1 MPa (2.22)

2.9 Definition of constraints

The re-evaluation of existing rock stress data help identifying constraints that in Chapter 3 will be applied in forced overcoring calculations. Because the analysis pinpoint the number of overcoring strains that are consistent with each of the constraints, it is possible to identify the set of constraints that, within statistical limits, fit the majority of data. This solution thus represents the most probable stress state at the Olkiluoto site.

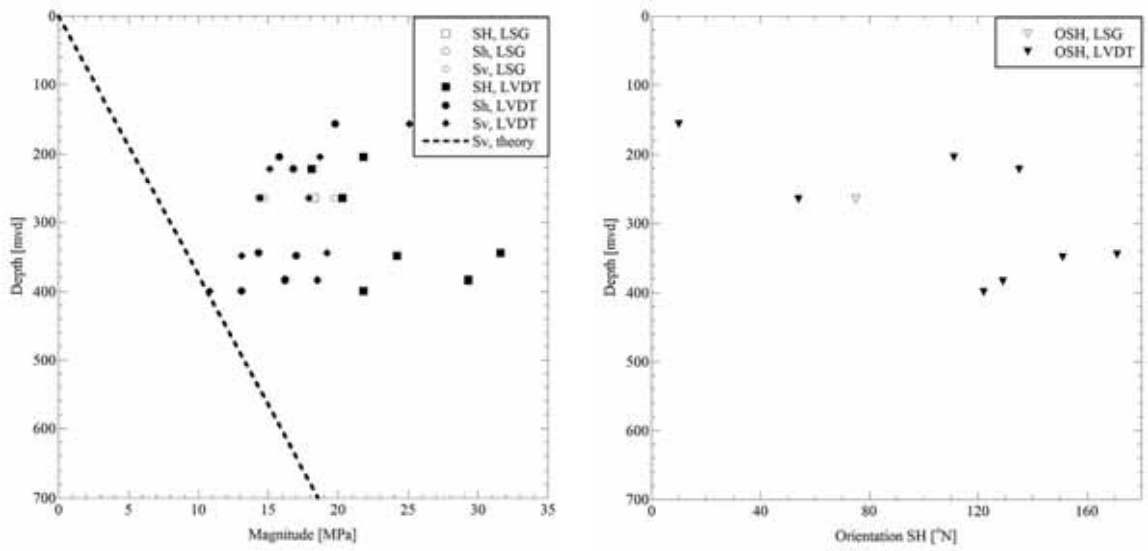

Figure 2-9. *Results from long strain gauges (Hakala 2010a) and LVDT tests (Hakala 2010b); horizontal stress magnitudes (left) and orientations (right). Both data sets represent the 2D solution without temperature correction and is valid between 150-400 mvd.*

The HF data provides constraints for both horizontal stress magnitudes as a function of depth and the orientation of the horizontal stresses. This is indeed beneficial as the overcoring data span over a considerable depth interval.

Moreover, because the hydraulic fracturing data clearly indicate that one principal stress is vertical, and the topographical effect negligible in the area, the vertical stress should be in close agreement with density measurements on cores.

As a result of that the previously and recently collected hydraulic stress data show slight differences and because the convergence, acoustic emission, LSG, and LVDT data are markedly different, the forced overcoring calculations were divided into four groups (a-e). However, common for both groups are constraints number 1 and 2, which are as follows:

1. One principal stress is vertical
2. σ_v is equal to the theoretical weight of the overburden (Eq. (2.1))

To investigate the correspondence between overcoring and hydraulic fracturing data, the following additional constraints are employed:

3a. Orientation of σ_H from previously collected HF data (Eq. 2.5)
4a. Magnitude of σ_h from previously collected HF data (Eq. 2.3)
3b. Orientation of σ_H from recently collected HF data (Eq. 2.8)
4b. Magnitude of σ_h from recently collected HF data (Eq. 2.6)

This implies that in the final step of the calculations, the magnitude of σ_H for the two methods may be compared. Conversely, the correspondence between overcoring and convergence+acoustic emission data are based on the following constraints:

3c. Orientation of σ_H from CM (Eq. 2.11)
3d. Orientation of σ_H from CM + AE (Eq. 2.14)
4d. Magnitude of σ_h from CM + AE (Eq. 2.12)

Finally, the result from the LSG and LVDT measurements are

3e. Orientation of σ_H from LSD + LVDT (Eq. 2.21)
4e. Magnitude of σ_h from LSD + LVDT (Eq. 2.19)

2.10 Influence of geology on overcoring results

As a result of the large scatter in orientations (and magnitudes) displayed by the overcoring data, the influence of geological structures such as dry and water-filled fractures, and foliation was investigated in the immediate vicinity of the overcoring locations. The study was limited to all structures within 2 m from the overcoring location and to investigate the orientation of the indicated stress field related to the orientation of the structure.

The effect of the geological structure on the local stress field is dependent on the stiffness of the structure relative to the surrounding rock mass. The analysis made hereafter is simplified and attempts to identify tests for which the principal stresses have oriented themselves after a pre-existing plane of weakness to become either parallel with or perpendicular to the plane. We conclude that the test is disturbed if the deviation of a principal stress direction is less than/equal to 15^o from that of a known plane of weakness. However, it should be noted that tests showing moderate influence of geological features will be omitted.

The results of the study are presented as a whole in Appendix 1 are involves stereographic plots of calculated principal stresses from overcoring tests, together with dip direction and dip of foliation and nearby-located fractures. In addition, plots with groups of nearby-located tests are also presented. The plots represent the lower hemisphere. Hereafter, we summarize the results from the study, involving both individual tests as well as groups of tests.

2.10.1 Drillhole ONK-PP170

In drillhole ONK-PP125, no information about foliation direction is available at the time of this report. The test at 223.92 mvd indicates that intermediate principal stress ($140^oN/16^o$) is similar to the dip and dip direction of a known fracture ($135^oN/30^o$).

2.10.2 Drillholes OL-KR10 and OL-KR24, 301-310 mvd

In drillhole OL-KR10, between 301 and 310 mvd, multiple pre-existing fractures exists. For both the test at 301.91 and at 310.76 mvd (σ_3 directed 345°N/50° and 288°N/64°, respectively), minimum principal stress is sub-parallel to existing fractures (355°N/53° and 284-311°N/26-52°).

For drillhole OL-KR24 and the test at 310.12 mvd, two foliation directions are present. The foliation directions (74-90°N/21-23° and 161-174°N/32-63°, respectively) are similar to the calculated direction of maximum and minimum principal stress (69°N/12° and 176°N/54°).

2.10.3 Drillhole OL-KR10, 319-333 mvd

At 319.01 mvd in drillhole KR10, two foliation directions are once again present (270°N/36° and 157°N/33°) that are very similar to calculated directions of maximum and minimum principal stress (151°N/36° and 270°N/34°).

2.10.4 Drillhole OL-KR24, 388-390 mvd

None of these tests indicate a principal stress direction aligned within 15° from a weakness plane.

2.10.5 Drillhole OL-KR10, 444-452 mvd

The test at 444.18 mvd indicates that maximum horizontal stress (51°N/19°) is nearly aligned with a fracture (48°N/7°), simultaneously as intermediate principal stress is sub-parallel with the foliation (148°N/20° and 156°N/37°, respectively).

The test at 452.91 mvd indicates that maximum horizontal stress is nearly aligned the foliation (88°N/23° and 90°N/31°, respectively).

2.10.6 Drillhole OL-KR10, 595-613 mvd

It should be noted that the amount of available information about foliation and existing fractures is more sparse compared with other intervals. Yet, we observe that the test at 595.46 mvd indicates that maximum horizontal stress (128°N/33°) is sub-parallel with the foliation (119-135°N/28-29°).

2.10.7 Conclusive remarks

Of the 21 technically reliable overcoring tests, 8 tests, or 38 %, indicate possible influence of pre-existing planes of weakness. However, removing these measurement points does not improve the precision of average orientation of maximum principal stress based solely on overcoring data. Nevertheless, given the crude nature of this analysis, the amount of potentially disturbed tests is regarded as high and it is conceivable that this may answer the observed scatter in principal stress orientations.

3 SEMI-INTEGRATION – FORCED OVERCORING CALCULATIONS

3.1 General

In the following, the re-evaluated overcoring strain data are forced to satisfy the constraints defined in Chapter 2.9. The objective is to identify the set of constraints that allow the maximum amount of overcoring strains in each drillhole and overcoring measurement levels. The calculations are based on two scales; (i) the single test scale (in which some tests may still involve ambiguous strains); and (ii) the measurement level scale (including only unambiguous strains and assuming that the group of tests sample the same stress field).

During the calculations, Chauvenet's criterion is used to detect outliers. The criterion implies that a strain gauge should be removed if the error between *a priori* and *a posteriori* strain reading is larger than:

$$\sqrt{\frac{\sum_{1}^{n}\left(\varepsilon_{i,apriori}-\varepsilon_{i,aposteriori}\right)}{n-1}} \tag{3.1}$$

where ε_i is overcoring strain number i and n is the number of tests. The first step to judge the consistency of a constraint involves a re-calculation of the stresses for both scales. These calculations give, with the aid of Chauvenet's criterion, a possibility to investigate the fit between *a priori* and *a posteriori* strains. This criterion also may be regarded as an estimate of the standard deviation of the strains (but only crudely as two sources of errors are mixed; those associated with measurement related uncertainties, and those of the interpretative model). For a set of strains subjected to a constraint, the constrained solution must indicate a standard deviation equal or less than that of the unconstrained solution. If the standard deviation is larger, the strain data are judged not consistent with the applied constraint. This approach is used at the measurement level scale.

For the single test scale, on the other hand, the problem may be is even-determined or just barely over-determined and as a result, the methodology becomes very sensitive. To judge the consistency of a constraint at the single test scale, the standard deviation derived from the unconstrained solution at the measurement level scale is used. This implies that uncertainties in the assumption of negligible stress variations in a group of tests is included also the single test scale, but it is judged that this additional uncertainty is significantly less than those arising from an even-determined or a barely over-determined equation system.

Throughout this chapter, the results of the various employments of constraints will be compared with the from the previous step, i.e. results from the application of constraint 1 will be compared with the results from the re-evaluated overcoring data, results from application of constraint 2 with the results from application of constraint 1 and so on. In Figure 3-1 and Figure 3-2, the results from the original and re-evaluated overcoring data are presented.

The results of the re-evaluation basically confirm the original interpretation with generally only minor changes in stress magnitudes and orientations. At both scales, σ_v and σ_h seem to be of the same order of magnitude. The σ_h- and σ_H-magnitudes are slightly underestimated respectively significantly underestimated compared with hydraulic fracturing data. The orientation of σ_H involves a considerable scatter but the average orientation, which may not necessarily represent the true orientation, is around 100°N for both scales.

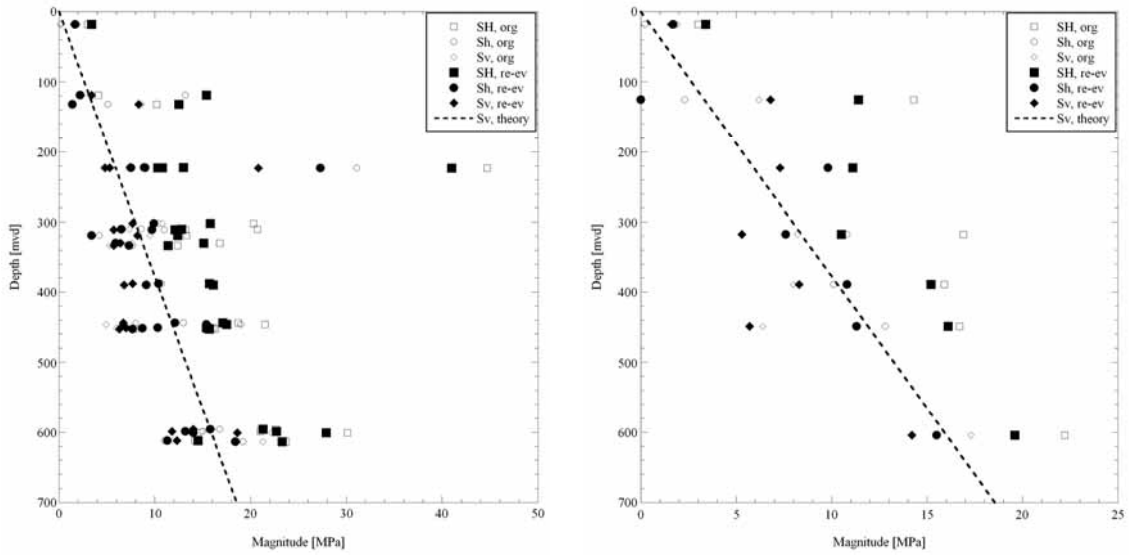

Figure 3-1. *Horizontal stress magnitudes from original interpretation and re-evaluation of overcoring data at the single test scale (left) and measurement level scale (right).*

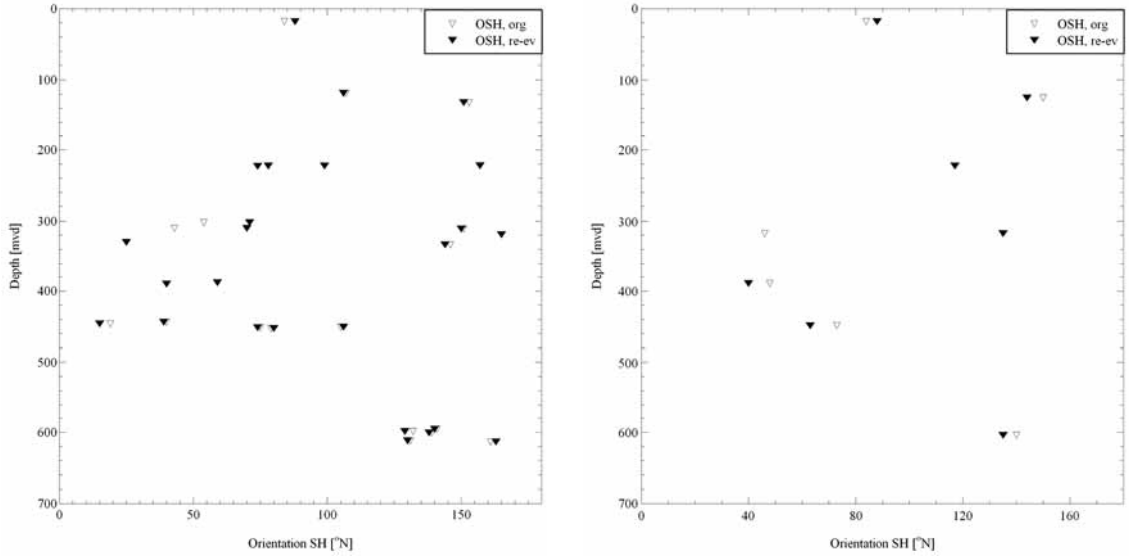

Figure 3-2. *Orientation of maximum horizontal stress from original interpretation and re-evaluation of overcoring data at the single test scale (left) and measurement level scale (right).*

3.2 Results from application of Constraint 1

Constraint 1 implies that re-evaluated overcoring strain data are forced to be consistent with a vertical principal stress.

3.2.1 Single test scale

At the single test scale, very minor effects are observed on both horizontal stress magnitudes and orientations (Figure 3-3). The average consistency of a vertical principal stress involves 95 % of the strain gauges. However, at this stage, several tests involve ambiguous strains in order to derive a solution, which is mostly pronounced for tests at level 7 (604 mvd). When excluding this level, the average consistency of application of Constraint 1 become 88 %.

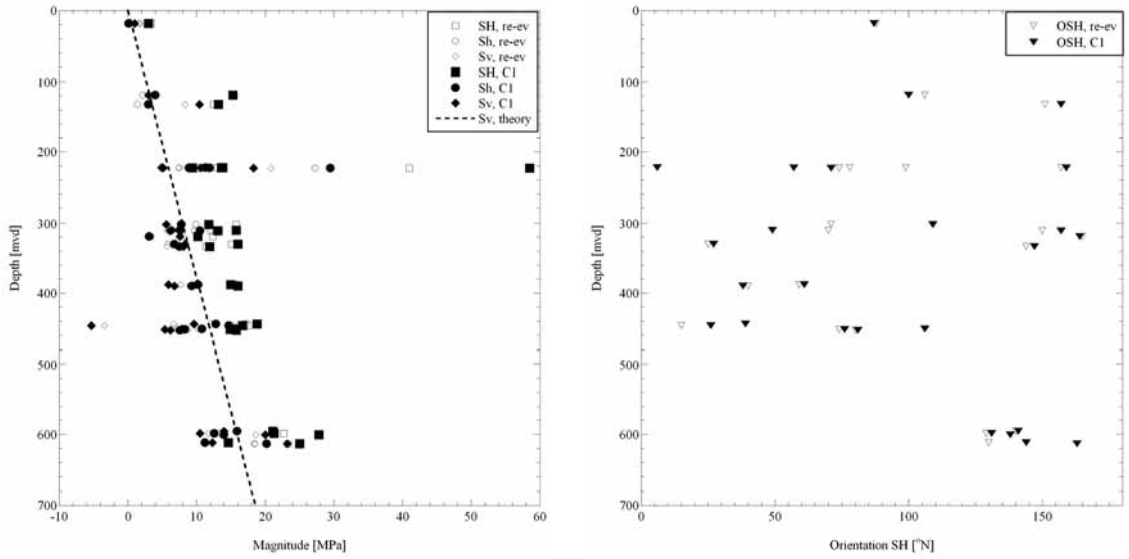

Figure 3-3. *Results from application of Constraint 1 and comparison with results from re-evaluation at the single test scale; stress magnitudes (left) and orientation of σ_H (right). Some ambiguous strains are included in the solutions.*

3.2.2 Measurement level scale

At the measurement level scale, the results between 100-300 mvd are clearly affected with a general increase in stress magnitudes (Figure 3-4). The average consistency of a vertical principal stress involves 75 % of the strain gauges.

3.3 Results from application of Constraints 1+2

Constraints 1+2 implies that re-evaluated overcoring strain data are forced to be consistent with a vertical principal stress equal to results from density measurements on cores ($\alpha_{v,theory}$ = 0.0265 MPa/m).

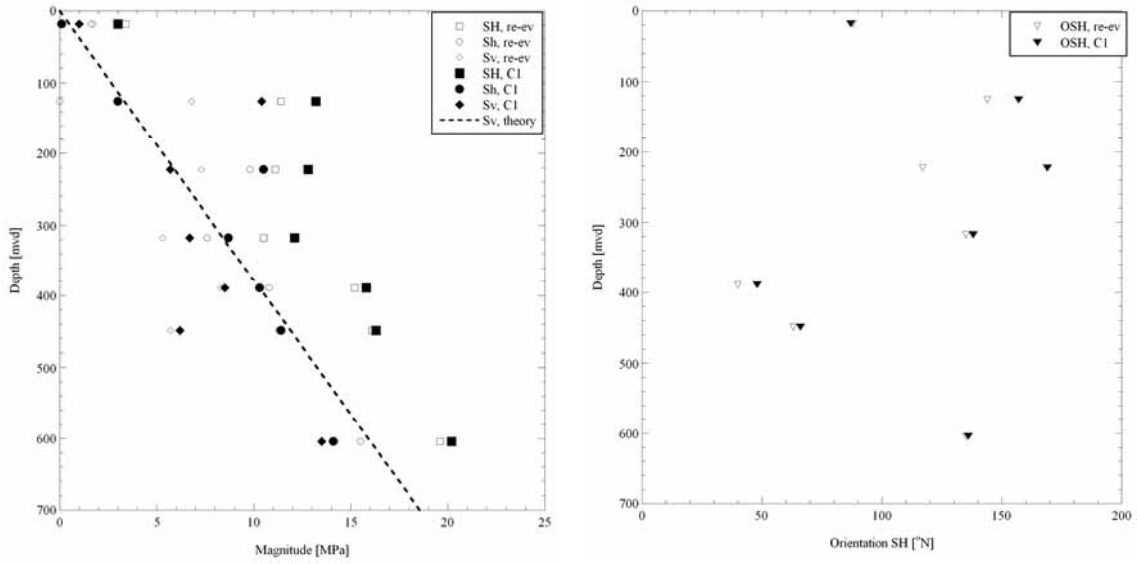

Figure 3-4. *Results from application of Constraint 1 and comparison with results from re-evaluation at the measurement level scale; stress magnitudes (left) and orientation of σ_H (right).*

3.3.1 Single test scale

The application of Constraints 1+2 indicates a consistency of 85 % of the strain gauges. However, also at this stage, several tests involve ambiguous strains in order to derive a solution, which is mostly pronounced for tests at Level 7 (604 mvd). When excluded, the average consistency of application of Constraint 1+2 becomes 77 %. Relatively minor changes in stress magnitudes and orientations are observed (Figure 3-5).

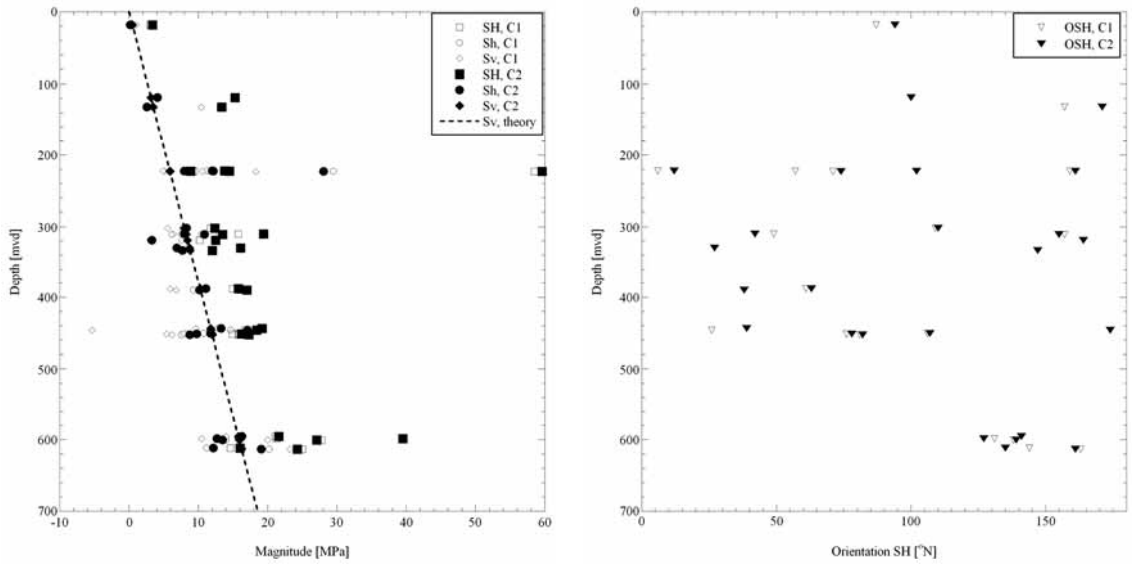

Figure 3-5. *Results from application of Constraints 1+2 and comparison with results from application of Constraint 1 at the single test scale; stress magnitudes (left) and orientation of σ_H (right). Some ambiguous strains are included in the solutions.*

3.3.2 Measurement level scale

Compared with the application of Constraint 1, the application of the additional Constraint 2 only has minor effects on stress magnitudes and orientations (Figure 3-6). The average consistency of a vertical principal stress involves 70 % of the strain gauges.

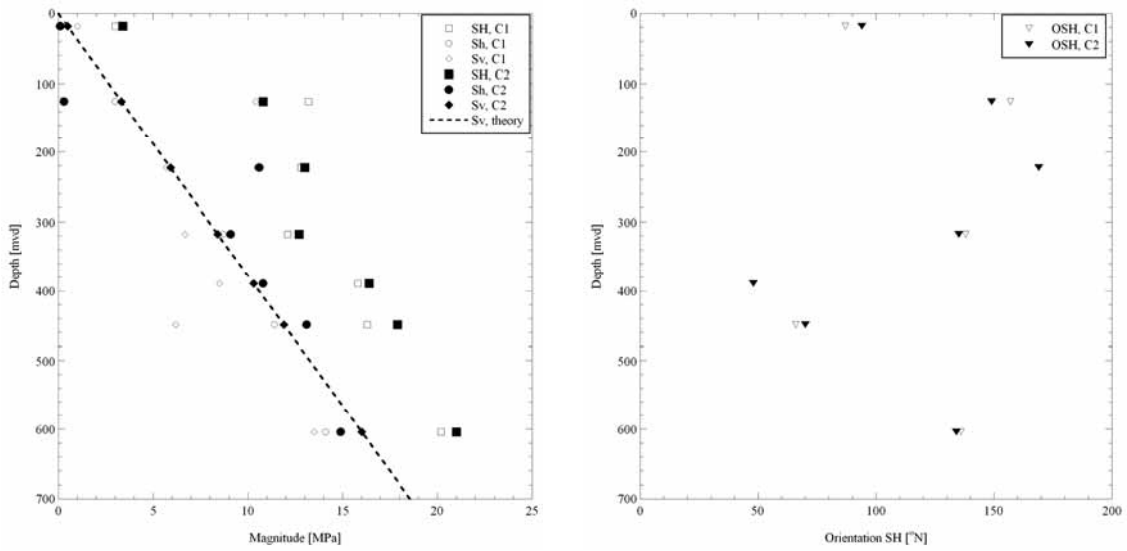

Figure 3-6. *Results from application of Constraints 1+2 and comparison with results from application of Constraint 1 at the measurement level scale; stress magnitudes (left) and orientation of σ_H (right).*

3.4 Results from application of Constraints 1+2+3a

Constraints 1+2+3a implies that re-evaluated overcoring strain data are forced to be consistent with a vertical principal stress equal to results from density measurements on cores ($\alpha_{v,theory}$ = 0.0265 MPa/m) and minimum horizontal stress magnitude from previously collected hydraulic fracturing data (92 ^{o}N).

3.4.1 Single test scale

The application of Constraints 1+2+3a indicates a consistency with 52 % of the strain gauges and involves only unambiguous data. The effect on stress magnitudes when fixing the orientation of σ_H at 92 ^{o}N is quite pronounced (Figure 3-7). Several tests now indicate a very small ratio σ_H/σ_h, which will be discussed further in Chapter 3.13.

3.4.2 Measurement level scale

Similar to the single test scale, the effect of fixing the orientation of σ_H at 92 ^{o}N has significant implications on stress magnitudes (Figure 3-8). At this scale, there is a general decrease in horizontal stress magnitudes, which is specially pronounced for the σ_H-magnitude. The average consistency involves 50 % of the strain gauges.

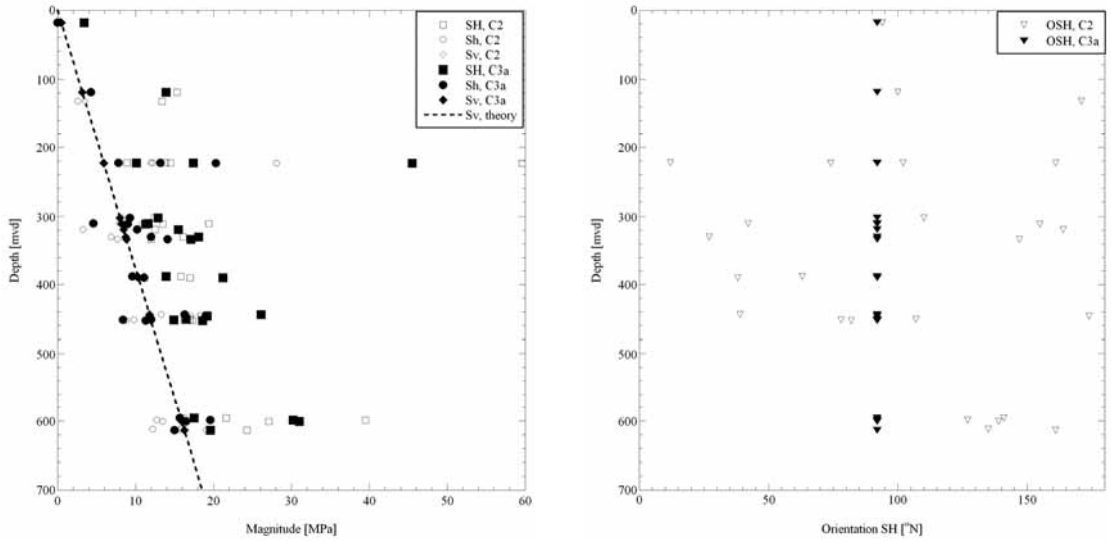

Figure 3-7. *Results from application of Constraints 1+2+3a and comparison with results from application of Constraints 1+2 at the single test scale; stress magnitudes (left) and orientation of σ_H (right).*

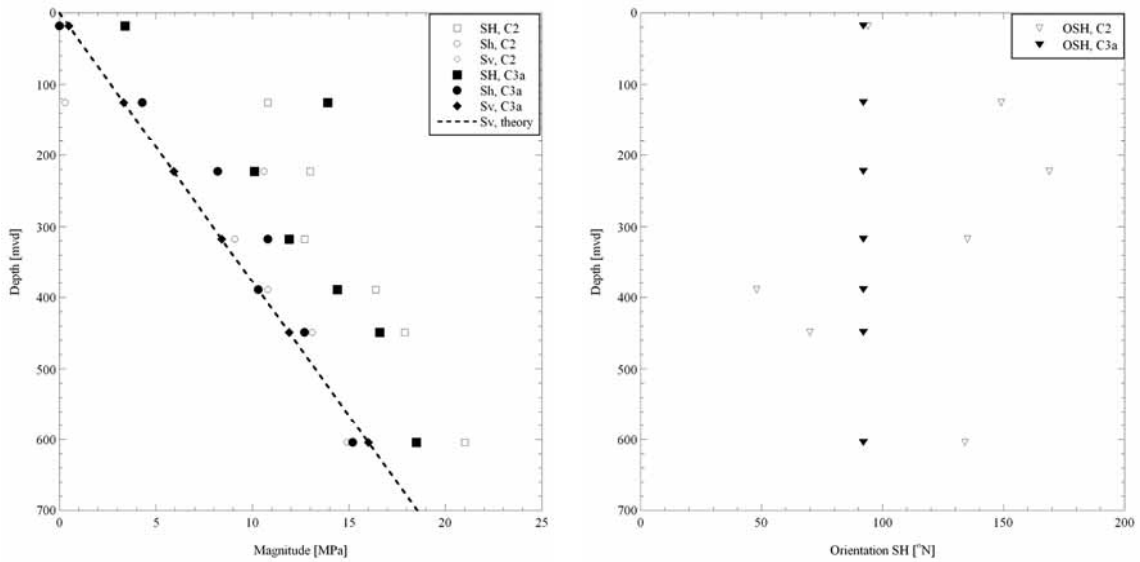

Figure 3-8. *Results from application of Constraints 1+2+3a and comparison with results from application of Constraints 1+2 at the measurement level scale; stress magnitudes (left) and orientation of σ_H (right).*

3.5 Results from application of Constraints 1+2+3a+4a

Constraints 1+2+3a+4a implies that re-evaluated overcoring strain data are forced to be consistent with a vertical principal stress equal to results from density measurements on cores ($\alpha_{v,theory}$ = 0.0265 MPa/m), minimum horizontal stress magnitude and orientation from previously collected hydraulic fracturing data (σ_h = 10.7+0.0321*(z-400) MPa and 92°N, respectively).

3.5.1 Single test scale

The application of Constraints 1+2+3a+4a indicates a consistency with 53 % of the strain gauges and involves only unambiguous data. The effect on stress magnitudes when also setting the σ_h-magnitude to equal the results from hydraulic fracturing data is quite pronounced (Figure 3-9). Similar to previous employment of Constraints 1+2+3a, several tests indicate a very small ratio σ_H/σ_h, which will be discussed further in Chapter 3.13. Note that the hydraulic solution is assumed valid between 200-850 mvd and no attempts were made to fit the most superficial data to Constraints 1+2+3a+4a.

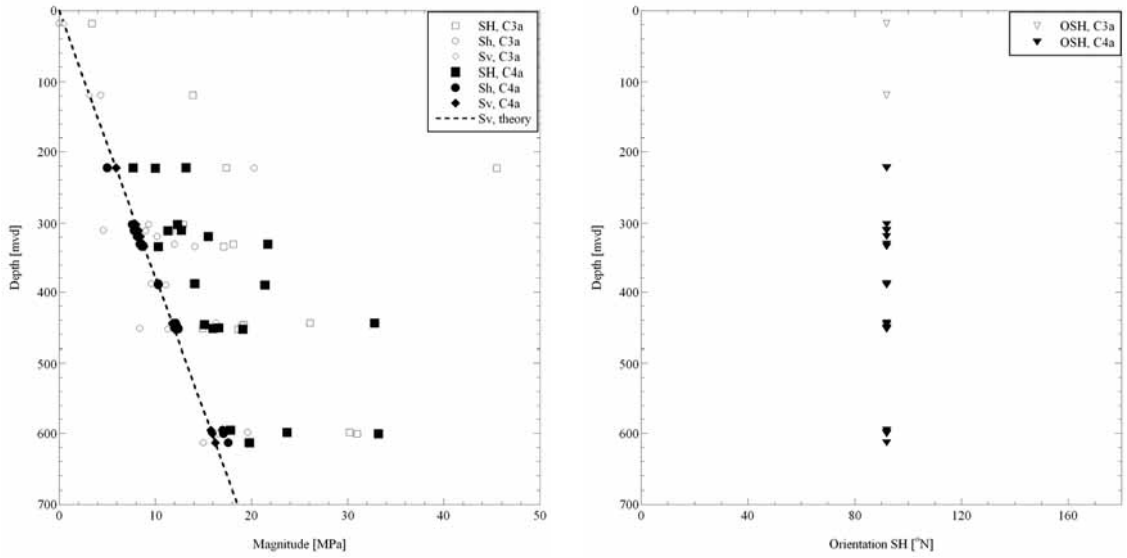

Figure 3-9. *Results from application of Constraints 1+2+3a+4a and comparison with results from application of Constraints 1+2+3a at the single test scale; stress magnitudes (left) and orientation of σ_H (right).*

3.5.2 Measurement level scale

Unlike the single test scale, the effect of fixing also the σ_h-magnitude according to previously collected hydraulic fracturing data has only moderate effect on the σ_H-magnitude (Figure 3-10). The average consistency of a vertical principal stress involves 56 % of the strain gauges. Similar to the single test scale, no attempts were made to fit the most superficial data to Constraints 1+2+3a+4a.

3.6 Results from application of Constraints 1+2+3b

Constraints 1+2+3a implies that re-evaluated overcoring strain data are forced to be consistent with a vertical principal stress equal to results from density measurements on cores ($\alpha_{v,theory}$ = 0.0265 MPa/m) and minimum horizontal stress magnitude from recently collected hydraulic fracturing data (78 ^{o}N).

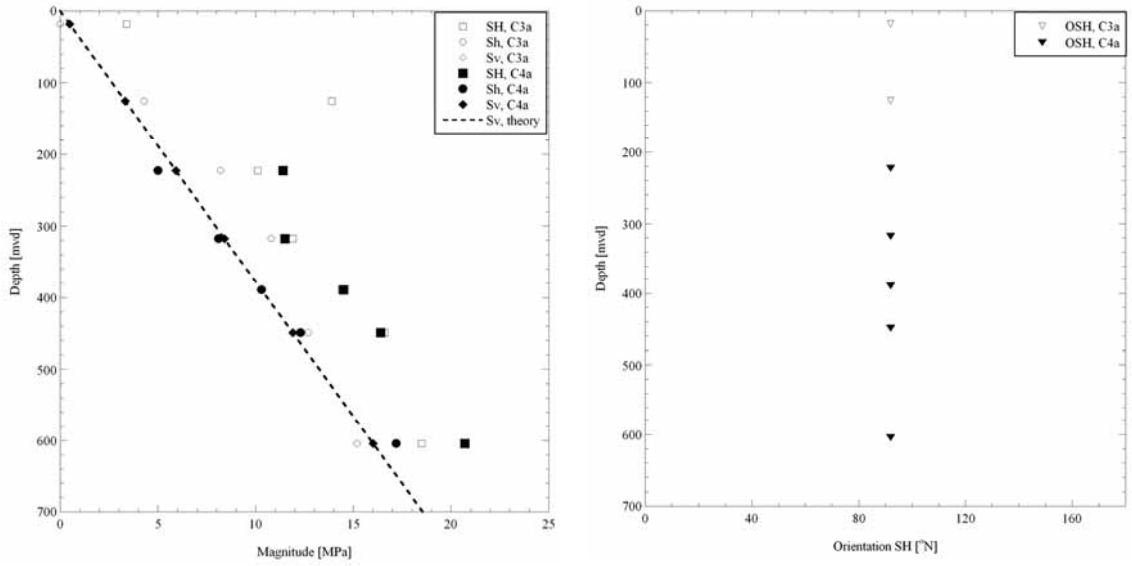

Figure 3-10. *Results from application of Constraints 1+2+3a+4a and comparison with results from application of Constraints 1+2+3a at the measurement level scale; stress magnitudes (left) and orientation of σ_H (right).*

3.6.1 Single test scale

The application of Constraints 1+2+3b indicates a consistency with 62 % of the strain gauges and involves only unambiguous data. The effect on stress magnitudes when fixing the orientation of σ_H at 80 ^{o}N is quite pronounced (Figure 3-11). Several tests now indicate a very small ratio σ_H/σ_h, which will be discussed further in Chapter 3.13.

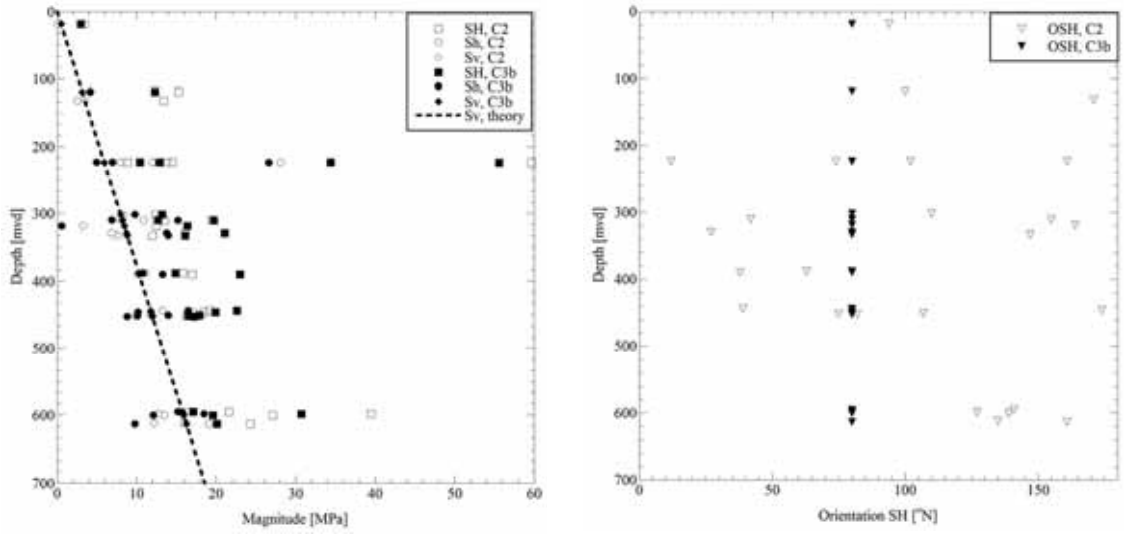

Figure 3-11. *Results from application of Constraints 1+2+3b and comparison with results from application of Constraints 1+2 at the single test scale; stress magnitudes (left) and orientation of σ_H (right).*

3.6.2 Measurement level scale

Similar to the single test scale, the effect of fixing the orientation of σ_H at 80 ^oN has significant implications on stress magnitudes (Figure 3-12). The average consistency involves 65 % of the strain gauges.

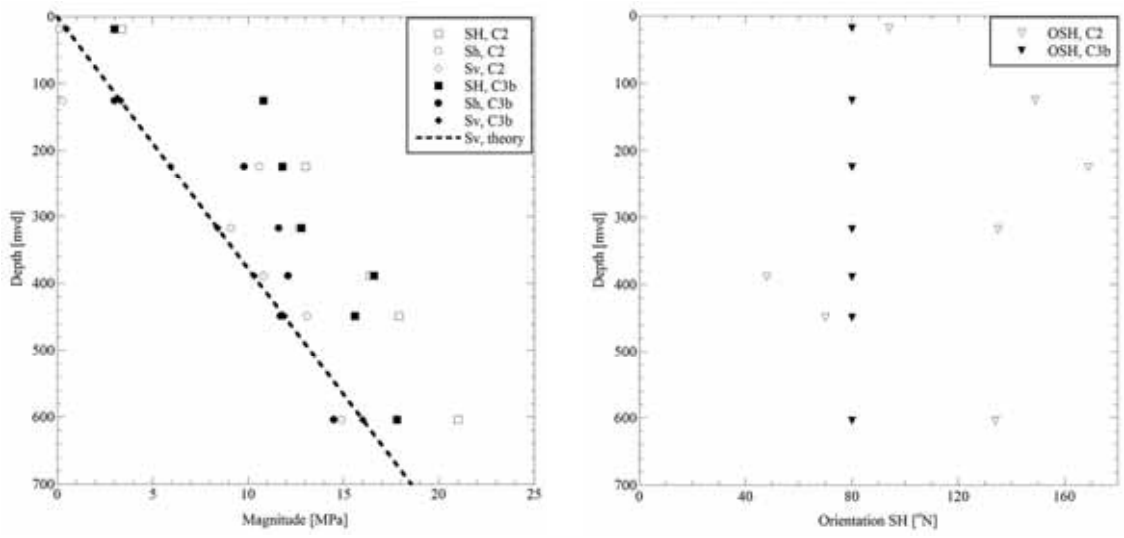

Figure 3-12. *Results from application of Constraints 1+2+3b and comparison with results from application of Constraints 1+2 at the measurement level scale; stress magnitudes (left) and orientation of σ_H (right).*

3.7 Results from application of Constraints 1+2+3b+4b

Constraints 1+2+3b+4b implies that re-evaluated overcoring strain data are forced to be consistent with a vertical principal stress equal to results from density measurements on cores ($\alpha_{v,theory}$ = 0.0265 MPa/m), minimum horizontal stress magnitude and orientation from previously collected hydraulic fracturing data (σ_h = 15.5+0.0360*(z-400) MPa and 78 ^oN, respectively).

3.7.1 Single test scale

The application of Constraints 1+2+3b+4b indicates a consistency with 41 % of the strain gauges and involves only unambiguous data. The effect on stress magnitudes when also setting the σ_h-magnitude to equal the results from hydraulic fracturing data is quite pronounced (Figure 3-13). Similar to previous employment of Constraints 1+2+3b, several tests indicate a very small ratio σ_H/σ_h.

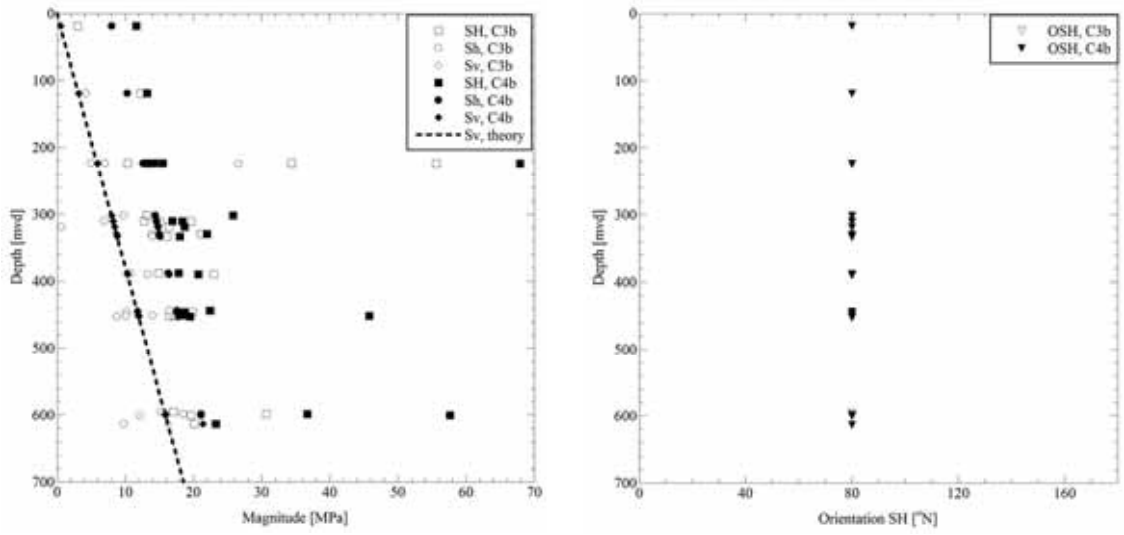

Figure 3-13. *Results from application of Constraints 1+2+3b+4b and comparison with results from application of Constraints 1+2+3b at the single test scale; stress magnitudes (left) and orientation of σ_H (right).*

3.7.2 Measurement level scale

Similar to the single test scale, the ratio σ_H/σ_h is close to one in the center of the interval (Figure 3-14), whereas more realistic ratios are observed at the upper and lower parts of the interval. The average consistency of a vertical principal stress involves 45 % of the strain gauges.

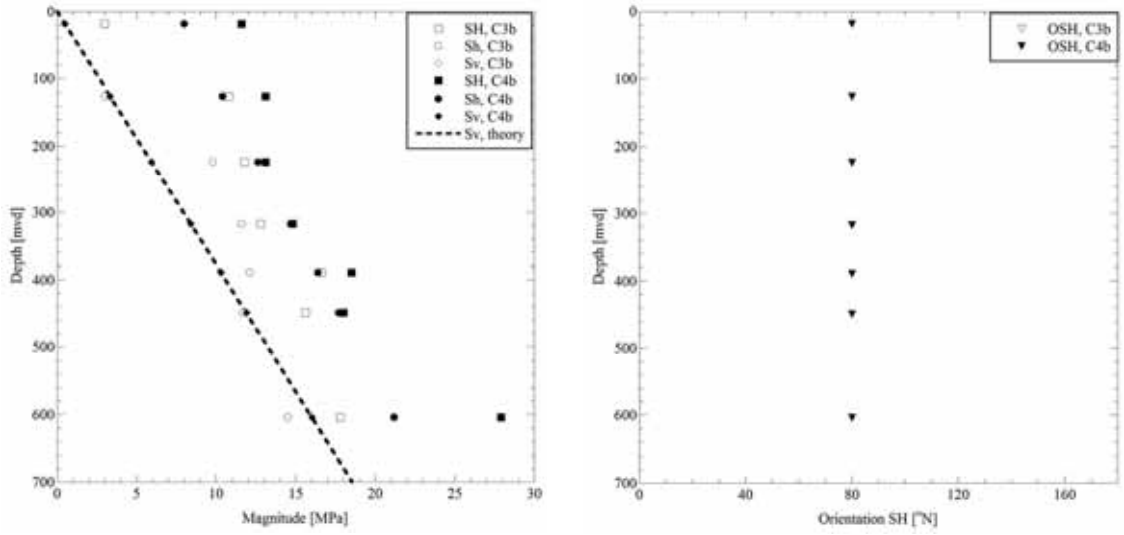

Figure 3-14. *Results from application of Constraints 1+2+3b+4b and comparison with results from application of Constraints 1+2+3b at the measurement level scale; stress magnitudes (left) and orientation of σ_H (right).*

3.8 Results from application of constraints 1+2+3c

3.8.1 Single test scale

The application of Constraints 1+2+3c indicates an overall consistency with 62 % of the strain gauges and involves only unambiguous data. The effect on stress magnitudes when setting the σ_H-orientation to 156 ^oN yields a relatively moderate effect as compared with Constraints 1+2 (Figure 3-15). However, for this alternative, nearly all tests indicate a ratio σ_H/σ_h close to unity.

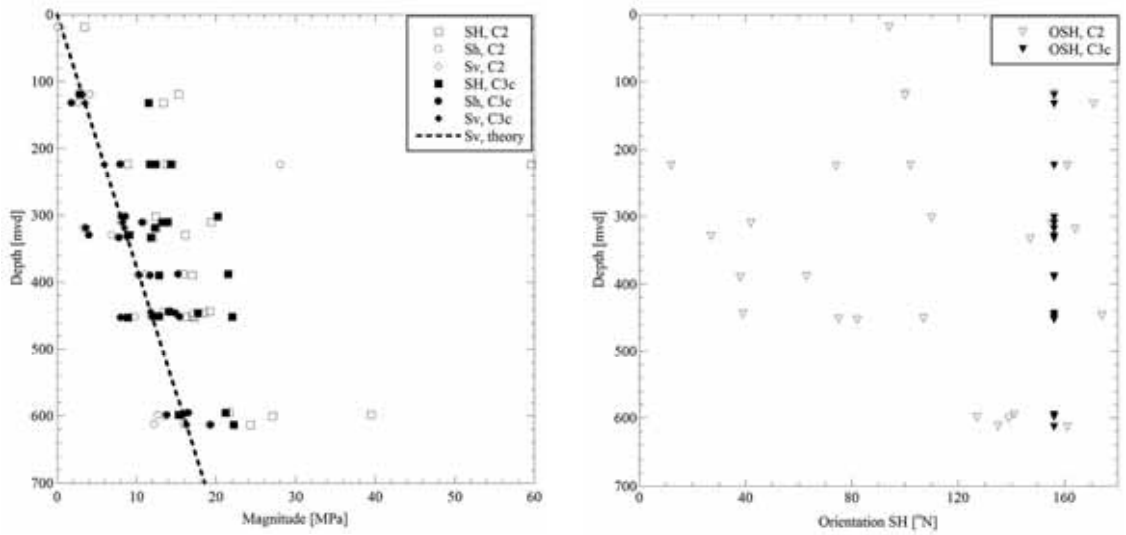

Figure 3-15. *Results from application of Constraints 1+2+3c and comparison with results from application of Constraints 1+2 at the single test scale; stress magnitudes (left) and orientation of σ_H (right).*

3.8.2 Measurement level scale

At the measurement level scale, the ratio σ_H/σ_h is somewhat larger compared to the single test scale. The non-linearity with depth is pronounced (Figure 3-16) The average consistency of a vertical principal stress involves 59 % of the strain gauges.

3.9 Results from application of Constraints 1+2+3d

Constraints 1+2+3d implies that re-evaluated overcoring strain data are forced to be consistent with a vertical principal stress equal to results from density measurements on cores ($\alpha_{v,theory}$ = 0.0265 MPa/m) and minimum horizontal stress magnitude from convergence and acoustic emission data (30 ^oN).

3.9.1 Single test scale

The application of Constraints 1+2+3d indicates a consistency with 47 % of the strain gauges and involves only unambiguous data. The effect on stress magnitudes when

fixing the orientation of σ_H at 30 ^oN is quite pronounced and two groups of data can be distinguished; those with small and with large difference between the σ_h- and σ_H-magnitudes, respectively (Figure 3-17). Some tests indicate a significant increase in σ_H-magnitude.

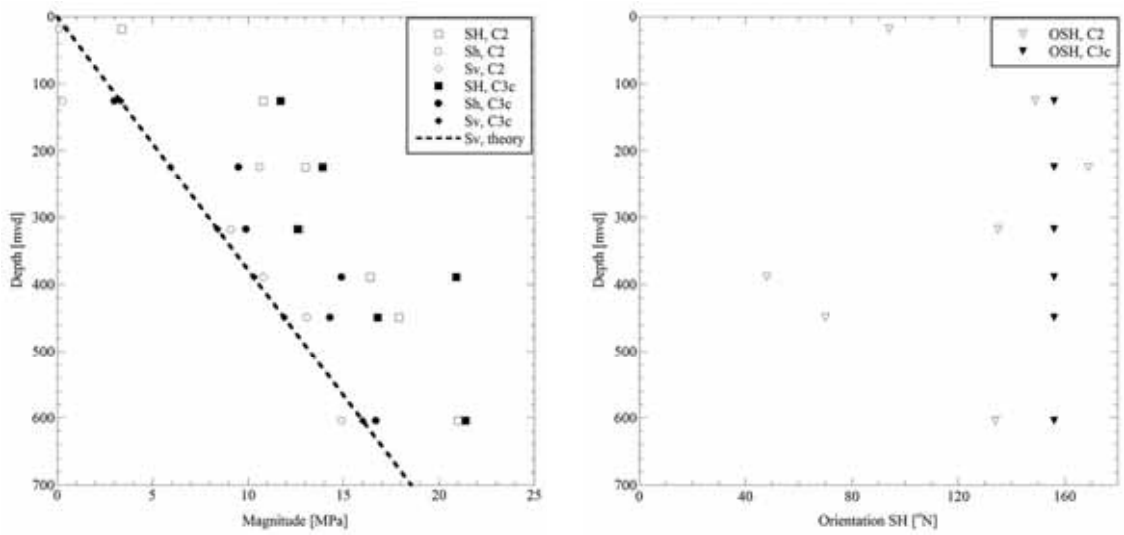

Figure 3-16. *Results from application of Constraints 1+2+3c and comparison with results from application of Constraints 1+2 at the measurement level scale; stress magnitudes (left) and orientation of σ_H (right).*

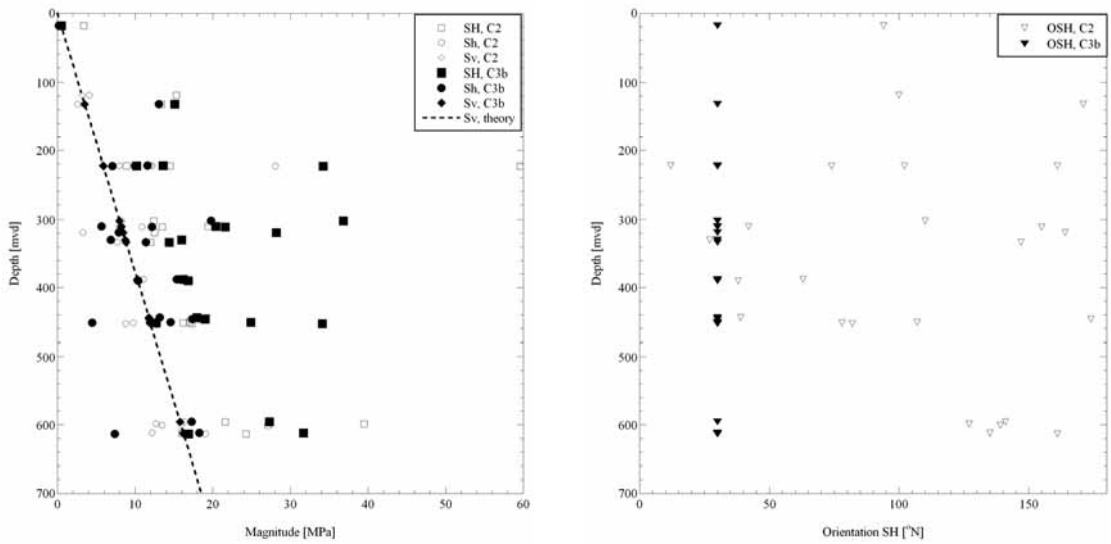

Figure 3-17. *Results from application of Constraints 1+2+3d and comparison with results from application of Constraints 1+2 at the single test scale; stress magnitudes (left) and orientation of σ_H (right).*

3.9.2 Measurement level scale

Unlike the single test scale, the effect of fixing the also the orientation of σ_H at 30 ^oN has only a moderate consequences on the stress magnitudes (Figure 3-18). The average consistency involves 47 % of the strain gauges.

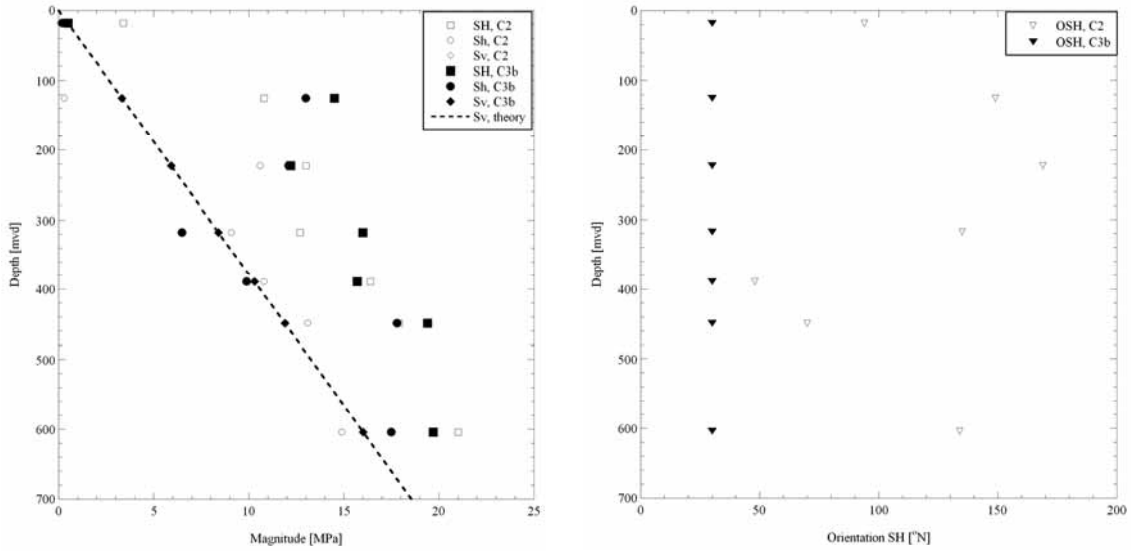

Figure 3-18. *Results from application of Constraints 1+2+3d and comparison with results from application of Constraints 1+2 at the measurement level scale; stress magnitudes (left) and orientation of σ_H (right).*

3.10 Results from application of Constraints 1+2+3d+4d

Constraints 1+2+3d+4d implies that re-evaluated overcoring strain data are forced to be consistent with a vertical principal stress equal to results from density measurements on cores ($\alpha_{v,theory}$ = 0.0265 MPa/m), minimum horizontal stress magnitude and orientation from convergence and acoustic emission data (σ_h = 9.1-0.0009*(z-400) MPa and 30^{o}N, respectively).

3.10.1 Single test scale

The application of Constraints 1+2+3d+4d indicates a consistency with 42 % of the strain gauges and involves only unambiguous data. The effect on stress magnitudes when also setting the σ_h-magnitude to equal the results from acoustic emission and convergence data is pronounced (Figure 3-19). As for the employment of Constraints 1+2+3a, two groups of data can be distinguished; those with small and with large difference between the σ_h- and σ_H-magnitudes, respectively. This will be discussed further in Chapter 3.13.

3.10.2 Measurement level scale

Unlike the single test scale, the effect of fixing also the σ_h-magnitude according to the results from acoustic emission and convergence data has only a moderate effect on the σ_H-magnitude (Figure 3-20). The average consistency of a vertical principal stress involves 42 % of the strain gauges.

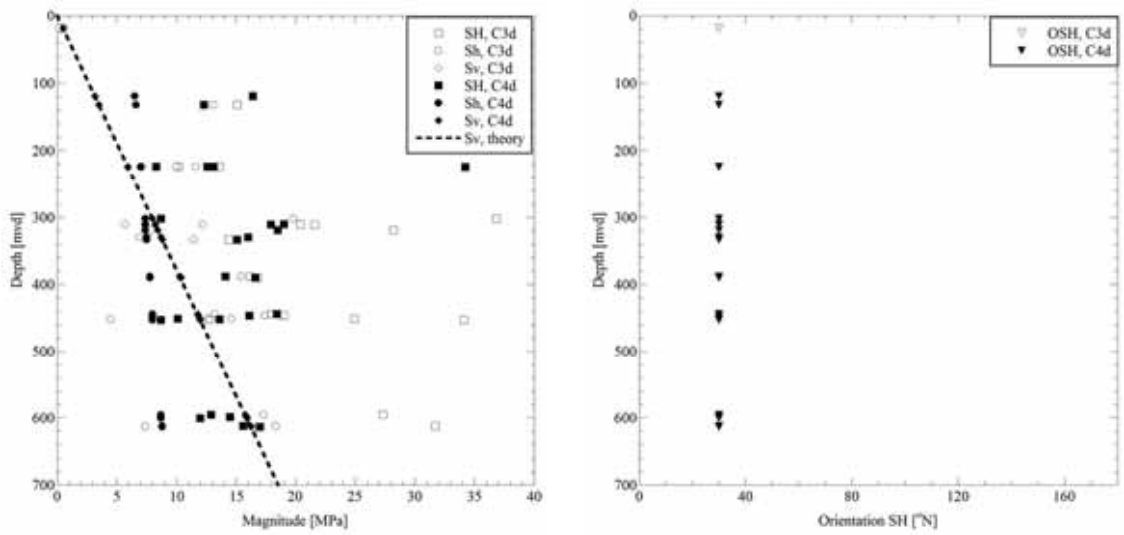

Figure 3-19. *Results from application of Constraints 1+2+3d+4d and comparison with results from application of Constraints 1+2+3d at the single test scale; stress magnitudes (left) and orientation of σ_H (right).*

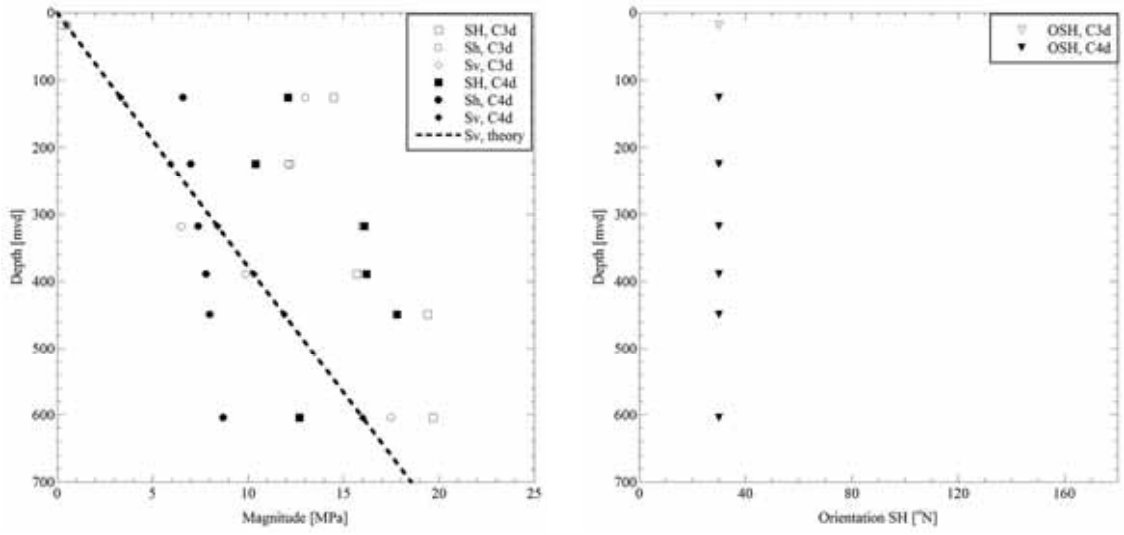

Figure 3-20. *Results from application of Constraints 1+2+3d+4d and comparison with results from application of Constraints 1+2+3d at the measurement level scale; stress magnitudes (left) and orientation of σ_H (right).*

3.11 Results from application of Constraints 1+2+3e

Constraints 1+2+3e implies that re-evaluated overcoring strain data are forced to be consistent with a vertical principal stress equal to results from density measurements on cores ($\alpha_{v,theory}$ = 0.0265 MPa/m) and maximum horizontal stress orientation from LSG and LVDT data (106 ^{o}N).

3.11.1 Single test scale

The application of Constraints 1+2+3e indicates a consistency with 52 % of the strain gauges and involves only unambiguous data. The effect on stress magnitudes when fixing the orientation of σ_H at 106 ^{o}N is relatively moderate but many tests indicate a small difference between the σ_h- and σ_H-magnitudes (Figure 3-21).

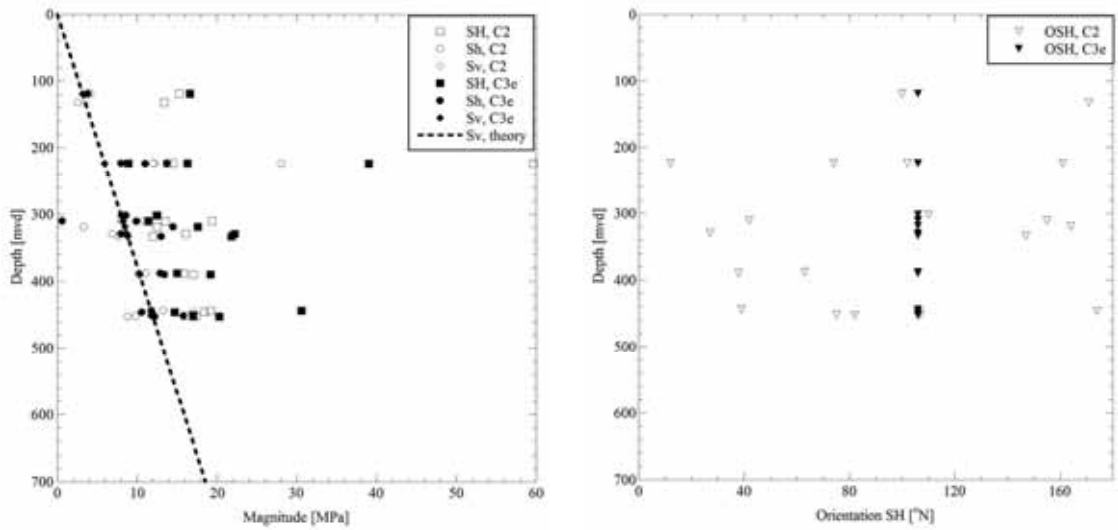

Figure 3-21. *Results from application of Constraints 1+2+3e and comparison with results from application of Constraints 1+2 at the single test scale; stress magnitudes (left) and orientation of σ_H (right).*

3.11.2 Measurement level scale

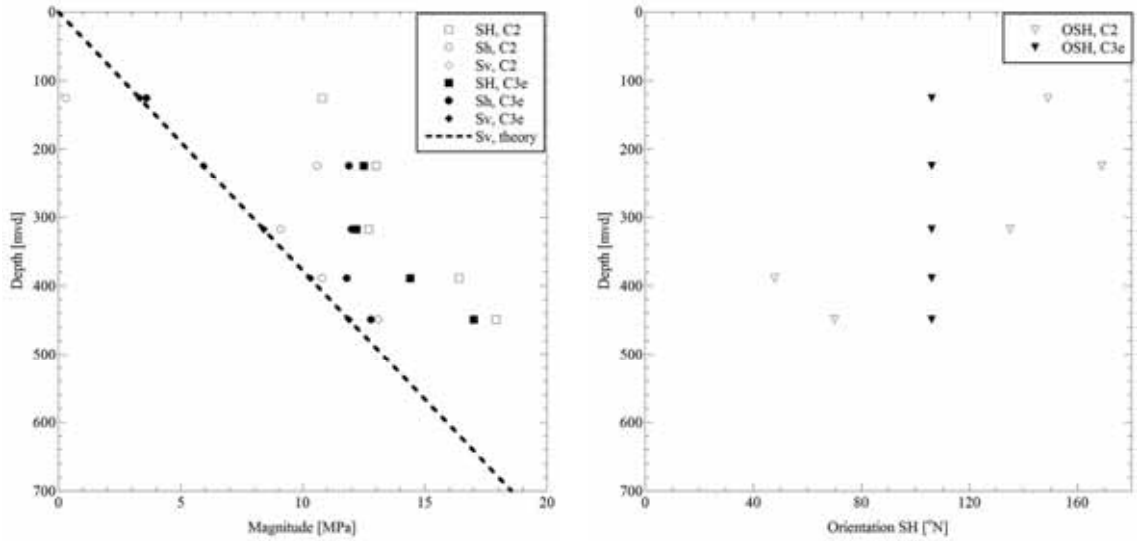

Figure 3-22. *Results from application of Constraints 1+2+3e and comparison with results from application of Constraints 1+2 at the measurement level scale; stress magnitudes (left) and orientation of σ_H (right).*

3.12 Results from application of Constraints 1+2+3e+4e

Constraints 1+2+3e+4e implies that re-evaluated overcoring strain data are forced to be consistent with a vertical principal stress equal to results from density measurements on cores ($\alpha_{v,theory}$ = 0.0265 MPa/m), maximum horizontal stress orientation and minimum horizontal stress magnitude from LSG and LVDT data (106 ^{o}N; 14.2 MPa (constant with depth)).

3.12.1 Single test scale

The application of Constraints 1+2+3e+4e indicates a consistency with 40 % of the strain gauges and involves only unambiguous data. The effect on stress magnitudes when also setting the σ_h-magnitude to equal the results from LSG and LVDT data is pronounced (Figure 3-21). Except for a few outliers, the results indicate a very small ration between maximum and minimum horizontal stress magnitudes. This will be further discussed Chapter 3.13.

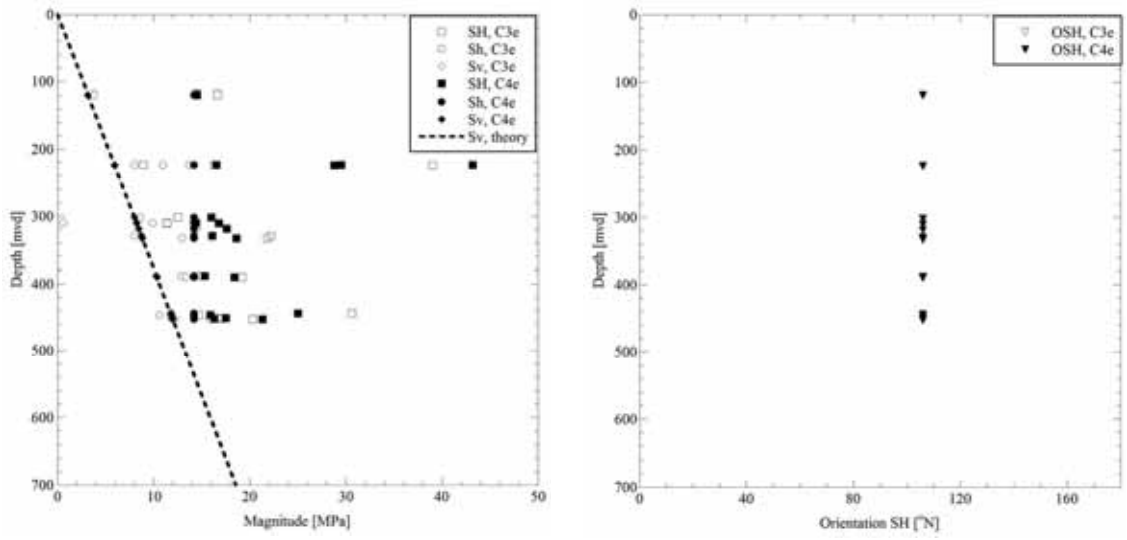

Figure 3-23. *Results from application of Constraints 1+2+3e+4e and comparison with results from application of Constraints 1+2+3e at the single test scale; stress magnitudes (left) and orientation of σ_H (right).*

3.12.2 Measurement level scale

The result at the measurement level scale is similar to the single test scale (Figure 3-22) with very small deviatoric stresses in the horizontal plane. The solution is consistent with 48 % of the strain gauges and involves only unambiguous data.

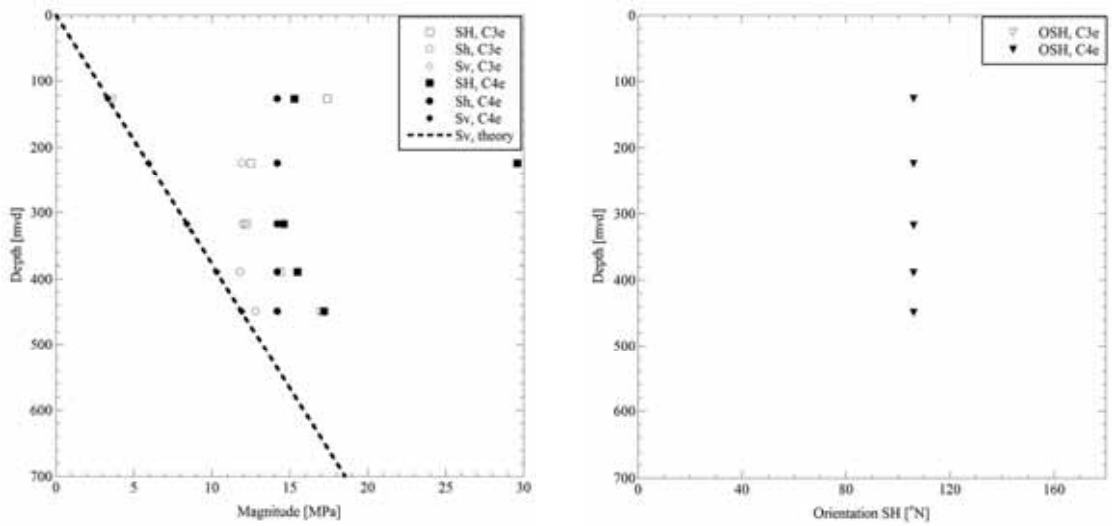

Figure 3-24. *Results from application of Constraints 1+2+3e+4e and comparison with results from application of Constraints 1+2+3e at the measurement level scale; stress magnitudes (left) and orientation of σ_H (right).*

3.13 Discussion and conclusions

3.13.1 General observations

The results from all forced stress calculations are summarized in Table 3-1 for the single test scale and in Table 3-2 for the measurement level scale. The corresponding equations for the stresses are given in Table 3.3. What is immediately apparent that there in some cases are large discrepancies in results between the two scales for a specific combination of constraints. This primarily concerns comparisons of the two first columns in Table 3-1 and Table 3-2. This is a result of that ambiguous strain gauges in some cases must be included in order to solve the stress at the single test scale. However, as the number of constraints is increased, the number of unknown parameters to be solved is reduced. This means that ambiguous strain data can be progressively removed as the number of constraints is increased. Application of Constraint 1 implies that only 4 unknown parameters are to be solved (σ_h-, σ_H-, σ_v-magnitudes, and orientation of σ_H). When adding Constraint 2, the number of unknowns is reduced to 3 (namely σ_h-, σ_H-magnitudes, and orientation of σ_H). Only two unknown parameters are left after application of Constraints 3a or 3d (namely σ_h-, σ_H-magnitudes), and finally only one unknown remains when applying Constraints 4a or 4d (namely σ_H-magnitude).

The degree of consistency of the overcoring data with Constraints 3a to 4e is regrettably not completely satisfactory. This outcome is interpreted as a result of: (i) large variability in results at the level scale due to measurement-related issues and/or true stress variation; and/or (ii) the constraints are not optimally defined.

Table 3-1. *Summary of results from forced overcoring calculations for each measurement level at the single test scale for the various constraints. Presentation of overcoring strain consistency for the various constraints.*

Lev.	Unambig. strains*	Constr. 1	Constr. 1+2	Constr. 1+2+ +3a	Constr. 1+2+ +3a+4a	Constr. 1+2+ +3b	Constr. 1+2+ +3b+4b	Constr. 1+2+ +3c	Constr. 1+2+ +3d	Constr. 1+2+ +3d+4d	Constr. 1+2+ +3e	Constr. 1+2+ +3e+4e
1	12	12 (100%)	8 (67%)	6 (50%)	-	10 (83%)	2 (17%)	0 (0%)	3 (25%)	0 (0%)	-	-
2	13	10 (77%)	10 (77%)	4 (31%)	-	4 (31%)	4 (31%)	10 (77%)	3 (23%)	0 (0%)	4 (31%)	1 (8%)
3	26	25 (96%)	22 (85%)	11 (42%)	8 (31%)	14 (54%)	13 (50%)	18 (69%)	16 (62%)	18 (69%)	12 (46%)	8 (31%)
4	46	41 (89%)	41 (89%)	28 (61%)	25 (54%)	29 (63%)	23 (50%)	35 (76%)	28 (61%)	23 (50%)	27 (59%)	18 (39%)
5	17	15 (88%)	14 (82%)	10 (59%)	10 (59%)	11 (65%)	9 (53%)	12 (71%)	12 (71%)	12 (71%)	6 (35%)	6 (35%)
6	45	34 (76%)	28 (62%)	27 (60%)	25 (56%)	30 (67%)	19 (42%)	26 (58%)	23 (51%)	14 (31%)	28 (62%)	26 (58%)
7	24	34 (142%)	32 (133 %)	15 (63%)	15 (63%)	16 (67%)	5 (21%)	12 (50%)	9 (38%)	9 (38%)	-	-
1-7	***183***	***171 (95%)***	***155 (85%)***	***101 (52%)***	***83 (53%)***	***114 (62%)***	***75 (41%)***	***113 (62%)***	***94 (47%)***	***76 (42%)***	***77 (52%)***	***59 (40%)***

Key: *See Chapter 2.2.1. Note that the application of Constraint 1 and Constraints 1+2 may involve ambiguous strain gauges.

Table 3-2. *Summary of results from forced overcoring calculations for each measurement level at the measurement level scale for the various constraints. Presentation of overcoring strain consistency for the various constraints.*

Lev.	Unambig. strains*	Constr. 1	Constr. 1+2	Constr. 1+2+ +3a	Constr. 1+2+ +3a+4a	Constr. 1+2+ +3b	Constr. 1+2+ +3b+4b	Constr. 1+2+ +3c	Constr. 1+2+ +3d	Constr. 1+2+ +3d+4d	Constr. 1+2+ +3e	Constr. 1+2+ +3e+4e
1	12	12 (100%)	8 (67%)	6 (50%)	-	10 (83%)	2 (17%)	0 (0%)	3 (25%)	0 (0%)	-	-
2	13	6 (46%)	6 (46%)	4 (31%)	-	7 (39%)	3 (23%)	8 (62%)	5 (38%)	0 (0%)	7 (39%)	3 (23%)
3	26	19 (73%)	20 (77%)	8 (31%)	10 (39%)	19 (73%)	11 (42%)	19 (73%)	13 (50%)	14 (54%)	16 (62%)	10 (39%)
4	46	34 (74%)	35 (76%)	29 (63%)	29 (63%)	24 (52%)	21 (46%)	33 (72%)	25 (54%)	25 (54%)	27 (59%)	23 (50%)
5	17	14 (82%)	14 (82%)	10 (59%)	10 (59%)	11 (65%)	8 (47%)	11 (65%)	12 (71%)	12 (71%)	9 (53%)	9 (53%)
6	45	31 (69%)	29 (64%)	26 (58%)	26 (58%)	31 (69%)	27 (60%)	19 (42%)	19 (42%)	18 (40%)	27 (60%)	26 (58%)
7	24	19 (79%)	18 (75 %)	14 (58%)	15 (63%)	17 (71%)	10 (42%)	18 (75%)	11 (46%)	7 (29%)	-	-
1-7	***183***	***135 (74%)***	***130 (71%)***	***97 (53%)***	***90 (57%)***	***119 (65%)***	***82 (45%)***	***108 (59%)***	***94 (47%)***	***76 (42%)***	***86 (59%)***	***71 (48%)***

Key: *See Chapter 2.2.1. Note that the application of Constraint 1 and Constraints 1+2 may involve ambiguous strain gauges.

Large variability in results at the measurement level scale is indeed apparent when studying Figure 3-1 and Figure 3-2, despite the attempts to remove ambiguous data. This variability effectively reduces the consistency of overcoring data with the applied constraints and would in fact do so independently of what type of constraint that is applied.

So far in this chapter, we have only discussed the degree consistency of the overcoring strains with the various constraints and now shift focus on the calculated stress functions (Table 3-3 and Table 3-4). At the single test scale, the stress magnitudes are relatively sensitive to the applied constraints. For tests with few unambiguous strains, this is to be expected as they represent an even-determined problem or just barely an over-determined problem. However, even when most strains gauges are excluded, many tests allow a relatively drastic change of result, yet with small strain differences and thus accepted as a solution. This implies, in theory, that stress calculations based solely on overcoring data may require additional information for reliable solutions. This, rather drastic, interpretation can be explained by the relatively large scatter of the measured strains in overcoring measurements combined with the mathematical algorithm used in the stress calculation, i.e. the least squares (LS) criterion. The LS criterion, in which the misfit is based on the l_2-norm, is known to be sensitive to non-distinct and atypical data (i.e. data with large variance and outliers, respectively; e.g. Parker and McNutt 1980). For such data, a more robust method is to use a misfit function based on the l_1-norm.

At the measurement level scale and when making linear regressions with depth at both single test and measurement level scale (Table 3-3 and Table 3-4), on the other hand, it is clear that the stress magnitudes close to repository depth (assumed to be at around 400 mvd) are not affected much by the various constraints. At the single test scale, σ_h and σ_H are generally in the range 10-14 and 17-21 MPa, respectively, whereas in the measurement level scale, σ_H is a few MPa lower; 15-17 MPa. This discrepancy is interpreted as a result of averaging, which means that peak values are smeared out in the average solution. Hence, for the overcoring data set as a whole, we can conclude that stress magnitudes and the consistency of strains are not altered significantly with the different constraints.

Another source of error is within the methodology itself and concern the methodology for evaluating the consistency. The methodology is based on Chauvenet's criterion and used the difference between measured (*a priori*) and calculated (*a posteriori*) strains as a crude estimate of standard deviation. However, the methodology is not straightforward as it mixes two sorts of errors; those associated with the measurement process and those associated with the interpretative model, which is not a completely rigorous method.

Table 3-3. *Summary of results from forced overcoring calculations; linear regression of data at the single test scale.*

Calc. step	σ_H [MPa]	σ_h [MPa]	σ_v [MPa]	Orientation of σ_H [^oN]
Re-eval.	17.0+0.0178*(z-400)	10.5+0.0176*(z-400)	8.7+0.0149*(z-400)	101+0.03*(z-400)
1	17.6+0.0137*(z-400)	10.9+0.0157*(z-400)	9.0+0.0164*(z-400)	99+0.06*(z-400)
1+2	19.3+0.0201*(z-400)	11.3+0.0168*(z-400)	10.6+0.0265*(z-400)	108+0.05*(z-400)
1+2+3a	19.1+0.0214*(z-400)	12.4+0.0212*(z-400)	10.6+0.0265*(z-400)	92+0.0*(z-400)
1+2+3a+4a	17.3+0.0346*(z-400)	10.7+0.0321*(z-400)	10.6+0.0265*(z-400)	92+0.0*(z-400)
1+2+3b	19.1+0.0100*(z-400)	11.6+0.0149*(z-400)	10.6+0.0265*(z-400)	80+0.0*(z-400)
1+2+3b+4b	26.0+0.0354*(z-400)	16.6+0.0225*(z-400)	10.6+0.0265*(z-400)	80+0.0*(z-400)
1+2+3c	15.1+0,0213*(z-400)	11.6+0,0251*(z-400)	10.6+0.0265*(z-400)	156+0.0*(z-400)
1+2+3d	21.4+0.0248*(z-400)	11.9+0.0149*(z-400)	10.6+0.0265*(z-400)	30+0.0*(z-400)
1+2+3d+4d	15.0-0.0046*(z-400)	7.8+0.0045*(z-400)	10.6+0.0265*(z-400)	30+0.0*(z-400)
1+2+3e	18.6+0.0039*(z-400)	11.8+0.0190*(z-400)	10.6+0.0265*(z-400)	106+0.0*(z-400)
1+2+3e+4e	18.7-0.0203*(z-400)	14.2+0.0000*(z-400)	10.6+0.0265*(z-400)	106+0.0*(z-400)

Key: z is the vertical depth.

Table 3-4. *Summary of results from forced overcoring calculations; linear regression of data at the measurement level scale.*

Calc. step	σ_H [MPa]	σ_h [MPa]	σ_v [MPa]	Orientation of σ_H [^oN]
Re-eval.	14.8+0.0242*(z-400)	10.5+0.0253*(z-400)	8.4+0.0151*(z-400)	101-0.02*(z-400)
1	15.7+0.0239*(z-400)	10.5+0.0230*(z-400)	8.7+0.0133*(z-400)	110-0.04*(z-400)
1+2	16.3+0.0274*(z-400)	11.1+0.0172*(z-400)	10.6+0.0265*(z-400)	110+0.05*(z-400)
1+2+3a	14.7+0.0213*(z-400)	11.2+0.0252*(z-400)	10.6+0.0265*(z-400)	92+0.0*(z-400)
1+2+3a+4a	15.0+0.0263*(z-400)	10.7+0.0321*(z-400)	10.6+0.0265*(z-400)	92+0.0*(z-400)
1+2+3b	14.8+0.0229*(z-400)	11.3+0.0252*(z-400)	10.6+0.0265*(z-400)	80+0.0*(z-400)
1+2+3b+4b	19.1+0.0254*(z-400)	16.6+0.0225*(z-400)	10.6+0.0265*(z-400)	80+0.0*(z-400)
1+2+3c	17.2+0.0208*(z-400)	12.7+0.0275*(z-400)	10.6+0.0265*(z-400)	156+0.0*(z-400)
1+2+3d	16.6+0.0276*(z-400)	13.2+0.0227*(z-400)	10.6+0.0265*(z-400)	30+0.0*(z-400)
1+2+3d+4d	14.5+0.0066*(z-400)	7.8+0.0045*(z-400)	10.6+0.0265*(z-400)	30+0.0*(z-400)
1+2+3e	14.7-0.0005*(z-400)	12.8+0.0237*(z-400)	10.6+0.0265*(z-400)	106+0.0*(z-400)
1+2+3e+4e	17.2-0.0122*(z-400)	14.2+0.0000*(z-400)	10.6+0.0265*(z-400)	106+0.0*(z-400)

Key: z is the vertical depth.

3.13.2 Result when setting a vertical principal stress equal to density measurements on cores (Constraints 1+2)

The results from all forced stress calculations (Table 3-1 and Table 3-2) clearly indicate that an overwhelming majority of collected overcoring strains are consistent with Constraint 1 and Constraints 1+2. Moreover, the application of the constraints only has a moderate effect on the stress magnitudes and orientations. Hence, we may state that the overcoring data do indicate that one principal stress is indeed vertical (or at least near vertical) and it is indeed in close agreement with the theoretical weight of the overburden rock mass ($\alpha_{v,theory}$ = 0.0265 MPa/m). This conclusion is made despite the fact that some ambiguous gauges were included at the single test scale.

3.13.3 Results when fixing also orientation of maximum horizontal stress (Constraints 1+2+3a to 3e)

When applying Constraints 1+2+3a to 1+2+3e, i.e. adding a fixed orientation of 92^o, 80^o, 156^o, 30^o, and 106 ^{o}N for σ_H, results are somewhat discouraging as the number of consistent strain gauges is quite similar for all the constraints. At the single test scale, the highest consistency is obtained for σ_H oriented 80^o and 156 ^{o}N (62 %), medium consistency for σ_H oriented 92^o and 106 ^{o}N (52 %), and the lowest consistency for σ_H oriented 30 ^{o}N, but still being as high as 47 %. At the measurement level scale, the highest consistency is obtained for σ_H oriented 80 ^{o}N (65 %), medium consistency for σ_H oriented 92^o, 156^o, and 106 ^{o}N (53 %, 59 %, and 59 %), and the lowest consistency for σ_H oriented 30^{o}N, but still being as high as 47 %. Thus, the results suggest that the overcoring data supports a σ_H-orientation most likely directed in the section NW to SW. However, given the small differences in consistency between the constraints it is far from conclusive.

To some extent, the observed small differences in consistency between the various constraints may be a result of that it is assumed that the constraints are constant with depths. Some variation is likely to exist, both in the vertical and horizontal direction, considering the complexity of the rock mass at the Olkiluoto site. Such variations would make it more difficult to differentiate two similar σ_H-orientations, such as 3a and 3b with σ_H oriented 80^o and 92 ^{o}N. It is not expected, on the other hand, that an *in situ* variation of the σ_H-orientation would lead to similar consistencies when σ_H is oriented 30 and 106 ^{o}N. Instead, this result speaks in favor of poor data quality that was not successfully identified and discarded during the raw data analysis of the overcoring data.

Shifting focus to stress magnitudes, multiple calculations show that the ratio σ_H/σ_h is unexpectedly small (and in a few cases unexpectedly large). This is a result of forcing the overcoring data to an orientation of σ_H that differ significantly from that of the conventional interpretation. In addition, the working procedure is to exclude data based on the Chauvenet's criterion, which does not involve consideration of the σ_H/σ_h-ratio. Instead, a solution is accepted even if the σ_H-magnitude exceeds the σ_h-magnitude by as little as 0.1 MPa, which in many cases may be considered unrealistic. Hydraulic fracturing data, for example, provide a measure of the minimum tangential stress around

the borehole and it cannot be less than zero, as this would lead to spontaneous tensile fracturing of the drillhole wall (and axial fractures has not been observed).

Conclusively, the application with constraints 1+2+3a to 3e leaves multiple questions still open and we proceed with constraints that involve also the σ_h-magnitude.

3.13.4 Results when fixing also magnitude of minimum horizontal stress (Constraints 4a-4d)

The inclusion of an additional constraint on the σ_h-magnitude shows, similar to the constraint on horizontal stress orientations, relatively drastic effects on the σ_H-magnitude on the single test scale but not as pronounced on the measurement level scale. Also in this calculation step, several tests indicate a very small difference between the horizontal stresses, whereas other displays a large difference.

Looking solely at the consistency, little can be said about the most likely stress state given by the overcoring data. Constraint 1+2+3a+4a has a slightly higher consistency (53 and 57 % at the single test and measurement level scales) compared to the other constraints (40-42 % and 42-48 %, respectively, at the single test and measurement level scales). Again, the consistency measure does not consider magnitude levels and to visualize better the consistency of magnitudes between overcoring data and other data sets, constrained σ_H-magnitudes of the overcoring data were analyzed with respect to the σ_H-magnitudes of the other data sets. Constrained overcoring solutions within ±5MPa of the other data sets are classified as fitting, whereas outside this interval as non-fitting (Table 3-5). Best results are obtained for overcoring data constrained towards new hydraulic data. For this case, 60 % of the individual overcoring tests fit within ±5MPa the σ_H-magnitude of the new hydraulic data (Equation 2.7). At the measurement level, the corresponding fit involves 86 %. A similar result is obtained for the solutions constrained with convergence and acoustic emission data, whereas it is somewhat lower for old hydraulic fracturing data. On the other hand, nearly none of the solutions constrained with LSGs and LVDTs fit the corresponding solution of these data (Equation 2.20). However, and similar to the previous section, the differences are not significant and the most likely state of stress from overcoring data cannot be distinguished.

Table 3-5. *Fit of σ_H-magnitudes between constrained overcoring data and other sources of data. Allowed discrepancy ±5MPa.*

Calc. step	Fit $\sigma_{H,\ Eq.\ (2.4)}$ [%]	Fit $\sigma_{H,\ Eq.\ (2.7)}$ [%]	Fit $\sigma_{H,\ Eq.\ (2.13)}$ [%]	Fit $\sigma_{H,\ Eq.\ (2.20)}$ [%]
1+2+3a+4a	48/60	-	-	-
1+2+3b+4b	-	60/86	-	-
1+2+3d+4d	-	-	64/71	-
1+2+3e+4e	-	-	-	8/0

Key: x/y denotes fitting data at single test scale/fitting data at measurement level scale.

3.13.5 Conclusions

Regrettably, the application of a semi-integration approach has not been fully satisfactory in that a reliable solution based on overcoring data combined with some other stress indicator. As it stands, multiple and widely different constraints show similar consistencies with respect to the number of accepted strain gauges or similarities in stress magnitudes. One of the most important factors of this outcome is likely the failure to reduce the initial pronounced scatter in the overcoring results in the re-evaluation. The remaining scatter in the re-evaluated data is judged too large to represent solely *in situ* stress variation; hence, measurement related errors are likely still present in the re-evaluated data set. A more in-depth analysis may to some extent decrease the scatter in data, but perhaps a more important issue is consideration to medium and large scale site geology, which is a topic that as been omitted in this study.

The large variability in results at the measurement level scale is visualized by the low consistency of overcoring strains with the various constraints, although they may also represent improperly defined constraints. Regrettably, low consistency prevails also at the single test scale, which may again indicate reduced data quality or limitations of the acceptance criteria and algorithm, as discussed in Chapter 3.13.1.

The exercise has however resolved a few important issues, which can be summarized as follows:

- The overcoring data suggest that one principal stress is vertical, or near vertical.
- The overcoring data suggest that the vertical component closely resembles measurements on cores.
- The overcoring data suggest that σ_H is most likely oriented in the section NW to SW.

4 CORE DISCING

4.1 Introduction

The core discing phenomenon appears when drill cores are retrieved from a rock mass that is subjected to a high *in situ* stress relative to its strength. The associated stress relief results in discing of the core, which may appear in a large variety of shapes. The core discing phenomenon was correlated to the stress field already in the late 1950ies (Hast 1958), and various researchers have since attempted to use them to predict the prevailing stress field.

The purpose of this chapter is to summarize all observed cases of core discing and attempt to correlate these firstly to specific rock types. A second objective is to investigate if they appear in specific rock blocks or are concentrated to certain geological features such as fracture zones. In addition, a third objective is to employ nomograms developed by Hakala (1999a, 1999b) to estimate *in situ* stress magnitudes.

4.2 Existing core discing data

In total, 48 observations of core discing have up to present been made at Olkiluoto. They are distributed over 16 drillholes and in the range between 30 to 1020 m drillhole length (mbl; Table A1-1 in Appendix 1). The discs are categorized depending on type or shape of the core ends according to the following groups:

1. Top surface concave, lower surface convex: **((**
2. Top surface concave, lower surface planar: **(|**
3. Top surface planar, lower surface convex: **| (**
4. Top surface convex, lower surface concave: **))**
5. Top surface convex, lower surface planar: **) |**
6. Top surface planar, lower surface concave: **|)**
7. Top surface planar, lower surface planar: **| |**
8. Top surface convex, lower surface convex: **) (**
9. Saddle shaped: S
10. Incomplete discs: A

The distribution of the core discing events with respect to disc shape (Figure 4-1) indicates that the majority of discs are incomplete followed by complete discs with planar-planar and concave-convex top and bottom surface, respectively, saddle-shaped discs and convex-concave top and lower surface. The other discs shapes seem to appear more sporadically.

The core discing data show a clear correlation with depth, i.e. the amount of discs with respect to depth is increasing (Figure 4-2). Note that in some cases, no information about the number of discs is available (see Appendix 1).

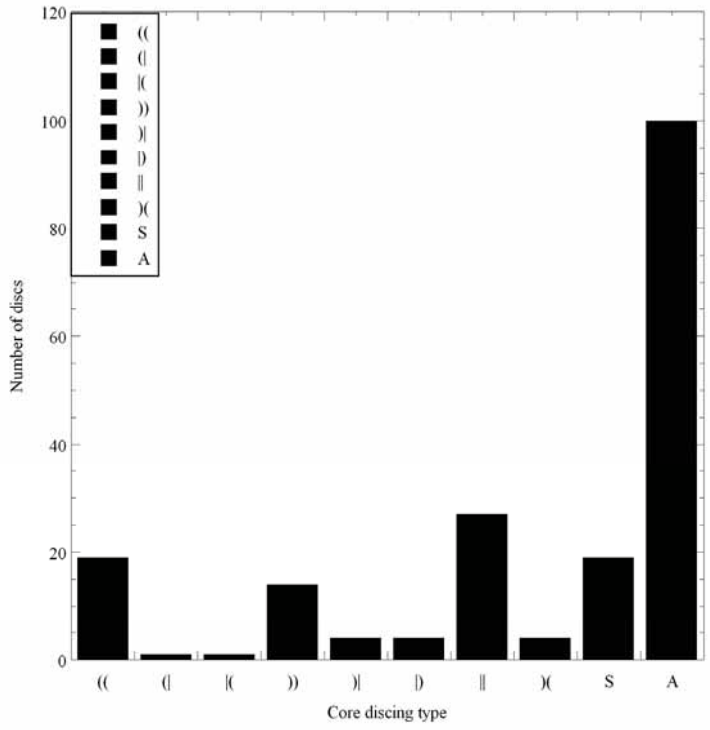

Figure 4-1. *Distribution of core discing with respect to type or shape of top and bottom surface of the discs.*

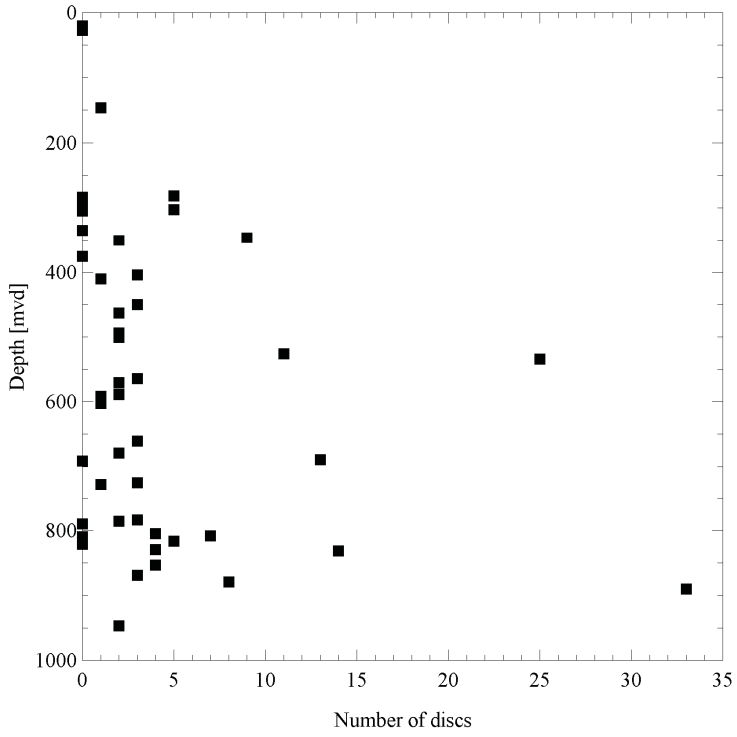

Figure 4-2. *Number of incomplete and complete discs as a function of depth.*

4.3 Correlation with rock types

In Figure 4-3, the corresponding rock type for each core discing group is displayed, indicating that pegmatitic granite (PGR) is the dominating domain for core discing phenomena (49 % of all observations), followed by veined gneiss (VGN; 24 %), (mica gneiss; 10 %), and diatexitic gneiss (DGN; 10 %). Only 6 % of the observations are made in mafic gneiss and tonalitic-granodioritic-granitic gneiss (MFGN and TGG, respectively).

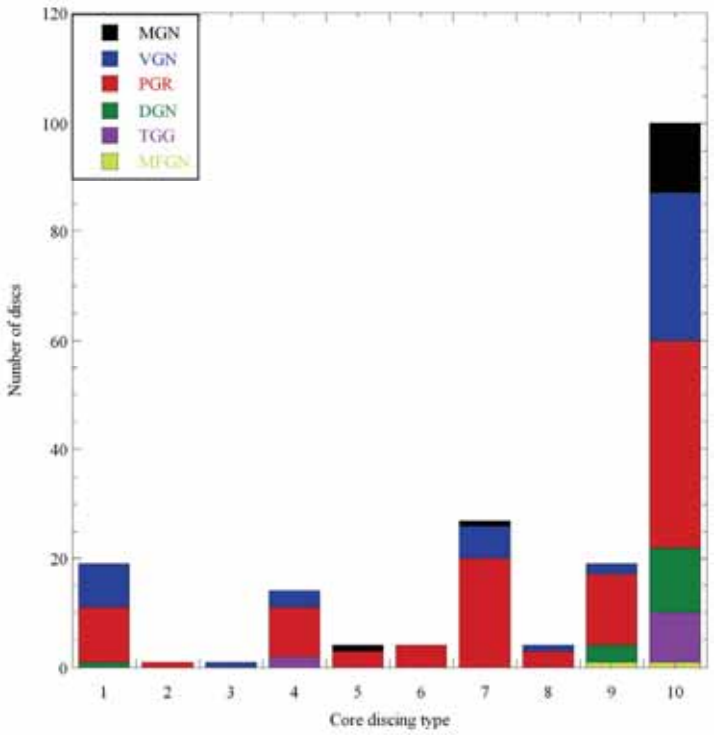

Figure 4-3. *Rock type distribution in each core discing group normalized with the total number of observed discs.*

4.4 Correlation with deformation zones

The correlation of observed core discing locations with known locations of existing deformation zones was made in two scales: (i) mapping of all structures up to 30 m of core discing locations; and (ii) mapping of all structures less than 10 m of core discing locations. In addition, the frequency of core discing events above and below known zones were investigated.

The results show that 17 core discing locations are within 30 m of existing deformation zones (Table 4-1). This implies that 35 % of all core discing locations are within 30 m from known locations of existing structures. However, only in three cases is the distance between the core discing locations less than 10 m from the existing deformation zone (6 %).

For the core discing locations within 30 m from a deformation zone, only one can be said to involve a relatively large number of discs (18 incomplete discs and one complete convex-convex disc). For the three cases where the core discing location is less than 10 m from a deformation zone, two cases indicate two single discs (both with one concave-convex and one planar-planar type), whereas the third involves one saddle-shaped disc and four incomplete discs. Because the material is limited, a statistical analysis is not warranted. It seems, however, that there is no correlation between core discing location and deformation zones. Note that this result does not preclude correlation between core discing locations and smaller scale structures.

Table 4-1. *Location of core discing observations relative to known deformation zones.*

CD observation			Geological structure			
Well	Start [m]	End [m]	Name	Start [m]	End [m]	Δz
OL-KR2	607.68	607.71	OL-BFZ002	603.6	604.6	3.6
OL-KR2	1019.72	1019.74	OL-BFZ104	1039.4	1040.9	20.4
OL-KR4	816.34	816.61	OL-BFZ130	791	792	25.0
OL-KR4	818.16	818.19	OL-BFZ130	791	792	26.7
OL-KR7	711.77	711.80	OL-BFZ002/099?	690.5	692	20.5
OL-KR7	711.77	711.80	OL-BFZ002/099?	696.3	697	15.1
OL-KR7	711.77	711.80	?	696.8?	700.3?	13.2
OL-KR11	314.69	314.79	?	300.6?	305.4?	11.7
OL-KR11	600.96	601.18	OL-BFZ002/099?	625.6	626.5	25.0
OL-KR12	523.48	523.50	OL-BFZ070	505	506	18.0
OL-KR12	760.03		OL-BFZ131	738.3	739.7	21.0
OL-KR12	760.03		OL-BFZ107	745.2	747.2	13.8
OL-KR16	154.95	155.19	OL-BFZ050/098	127.5	130.2	26.2
OL-KR19	487.14	487.41	OL-BFZ002	464.7	465.3	22.3
OL-KR19	487.14	487.41	OL-BFZ002	476.7	477.9	10.0
OL-KR19	487.14	487.41	OL-BFZ002	484.6	485.9	2.0
OL-KR23	407.17	411.52	OL-BFZ098	427.6	428.5	18.7
OL-KR23	415.46	420.26	OL-BFZ098	427.6	428.5	10.2
OL-KR23	446.64	447.64	OL-BFZ098	427.6	428.5	19.1
OL-KR23	450.15		OL-BFZ098	427.6	428.5	22.1
OL-KR24	384.17	387.10	OL-BFZ080	397	397.9	11.8
OL-KR24	388.46	388.48	OL-BFZ080	397	397.9	9.0

When considering the frequency of core discing events above and below known zones an interesting observation can be made. In drillhole OL-KR1, 46 discing events are reported between 784 and 969 mbl, i.e. below zone OL-BFZ002. This zones crosses drillhole OL-KR1 at 611.0-618.0 and 641.0-642.2 mbl and no additional zones have been identified below 642 mbl. In drillhole OL-KR2, 33 discing events are reported between 607 and 1020 mbl, which is a domain constrained by zone OL-BFZ002 (603.6-604.6 mbl) and zone OL-BFZ104 (1039.4-1040.9 mbl). In drillhole OL-KR4, 10 discing events are reported between 816-854 mbl, which is below zone OL-BFZ002 (791.0-792.0 mbl) and no additional zones have been identified below 792 mbl. In drillhole OL-KR11, 25 discing events are located 25 m above zone OL-BFZ002 (located at 625.6-626.5 mbl), two in between zones OL-BFZ002 and OL-BFZ105 (located at 895.5-896.0 mbl), and 18 are located some 60 m below zone OL-BFZ105. In addition, discing events in drillhole OL-KR7, OL-KR12, and OL-KR19 are also located fairly close to zone OL-BFZ002 (located about 20, 35, and 10 m away from the zone). Hence, a common factor for many of the drillholes with core discing events seems to be zone OL-BFZ002, which may be worth continued studies. It should be noted that this suggestion is made without considering local geology at these discing locations.

4.5 Estimation of stress magnitudes from core discing data

Information on core discing can be used to estimate the virgin stress state. A methodology for this was described by Hakala (1999a, 1999b, 2000). The methodology is based on the assumption that core discing is caused by pure tensile failure. Furthermore, continuous, homogeneous, linear-elastic and isotropic conditions (up to the point of failure) must be assumed. Hakala (1999a) described both a computer program for analysing core discing and the acting stresses, as well as nomograms for quick assessment of the stress state. The nomograms have the following limitations (compared to the computer code):

- one principal stress must be aligned with the drillhole;
- Poisson's ratio (ν) must be 0.25; and
- the stress ratio σ_h / σ_H must be 0.25, 0.50, 0.75, or 1.0.

According to Hakala (1999a), an accurate determination of the stress state requires information on core discing both from normal coring and overcoring (hollow core; ring discing). Also, the numerical model used for developing the methodology had fairly large zones, resulting in inaccurate results for thin discs (spacing of 10 mm or less; Hakala 2004).

All observed core discing from Olkiluoto was of the type normal core, with one exception as noted above. Based on these uncertainties, as well as the sparse information on core discing geometry available, it was not deemed justifiable to use the numerical code. Hence, only the nomograms were used in the following preliminary stress estimation.

Direct and indirect tensile strength in different rock types at the Olkiluoto site has been determined (Andersson et al. 2007). It should be noted that the determined direct and

indirect tensile strength are different. The indirect testing configuration may be more closely reflect the tensile strength governing core discing, these are thereby used, shown in Table 4-2. Furthermore, given the inherent uncertainties in using the nomograms for stress estimation (as described above), the possible differences in direct and indirect tensile strength values are judged to be of relatively lesser importance.

Table 4-2. *Indirect tensile strength of different rock types at the Olkiluoto site. (from Andersson et al. 2007)*

Rock type	Indirect tensile strength [MPa]
VGN	11.7
DGN	10
MGN	12.2
TGG	14.4
PGR	5.4

Stresses from Andersson et al. (2007):

$\sigma_H = 7.5 + 0.0315\ z$ (1)

$\sigma_h = 2.5 + 0.024\ z$ (2)

$\sigma_v = 0.0225\ z$ (3)

The σ_h/σ_H - ratio for each location was calculated, and then two different nomograms were used. To estimate the *in situ* stresses, the ratios σ_t/σ_H and σ_v/σ_H are used together with the observed spacing of core discing. These two ratios are dependent on each other; hence, the maximum horizontal stress cannot be determined directly. Using the nomograms, a trial value was first determined for σ_t/σ_H from observed disc spacing. This value was then used to determine a corresponding value on σ_v/σ_H. The value on the maximum horizontal stress, σ_H, was calculated from both these ratios and compared. If the values differed, a new trial value was chosen and the procedure repeated until the value of σ_H converged. An example is shown in Figure 4-4 where 13 mm disc thickness yields a value of 0.41 for the ratio σ_t/σ_H and a value of 0.19 for σ_v/σ_H.

For most of the measurements the values never converged. The obtained results are presented in Table 4-3.

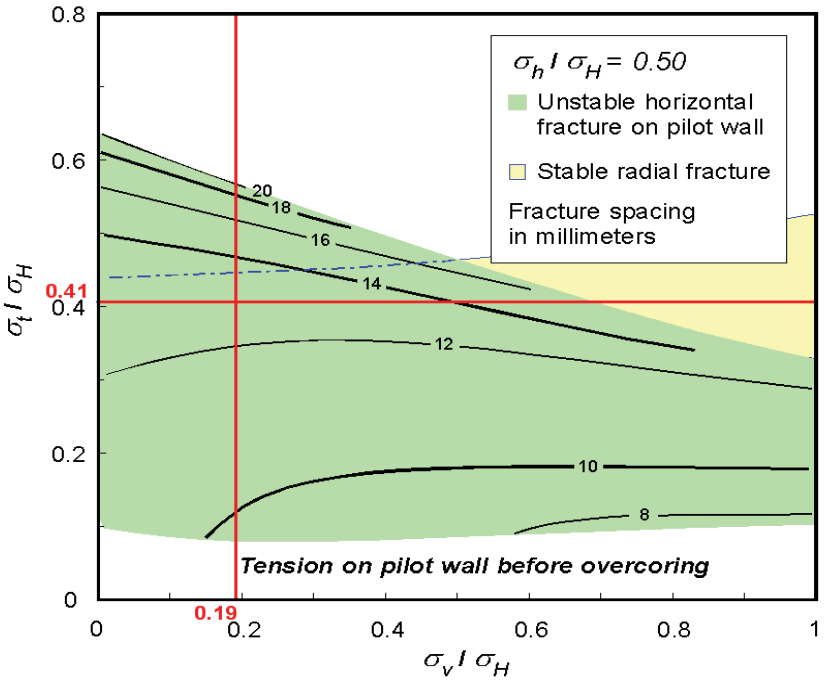

Figure 4-4. *Nomogram (from Hakala, 1999a) for estimating in situ stress from observed core discing; example of procedure:* $\sigma_h/\sigma_H = 0.50$, $\sigma_t = 14$ *MPa, disc thickness = 13 mm,* $\sigma_v = 6.3$ *MPa, yields* $\sigma_t/\sigma_H = 0.41$, $\sigma_v/\sigma_H = 0.19$, *from which* $\sigma_H = 34$ *MPa.*

Table 4-3. *Stress estimation from core discing using nomograms by Hakala (1999a).*

Drillhole	Rock type	Average depth [m]	σ_h/σ_H	Disc thickness [mm]	σ_t/σ_H	σ_v/σ_H	σ_H [MPa]
OL-KR11	PGR	279.71	0.56	30	0.24	0.28	22.50
OL-KR19	MGN	352.94	0.59	20	0.23	0.15	53.04
OL-KR11	VGN	526.22	0.63	30	0.24	0.24	48.75
OL-KR2	DGN	680.42	0.65	37	0.26	0.40	38.46

4.6 Conclusions

The dominating disc type at the Olkiluoto site is the incomplete disc, followed by complete discs with planar-planar, concave-convex, saddle-shaped, and convex-concave discs. The other discs shapes seem to appear more sporadically.

It is not evident that the discing events can be correlated with existing and larger deformation zones, although discing events may possibly be correlated to zone OL-BFZ002. Note that the analysis has only been made with respect to the major deformation zones, which does not preclude that discing events may be correlated to smaller scale zones. However, what is evident, is that the majority of discing events

occur in pegmatitic granite (PGR; 49 % of all observations). Events in other rock types are significantly less frequent (24 % in veined gneiss; 10 % in mica gneiss; 10 % in diatexitic gneiss; and 6 % in mafic gneiss and tonalitic-granodioritic-granitic gneiss).

The derived horizontal stress magnitudes using the nomogram approach show a relatively scattered result. The result for pegmatitic granite at 280 mvd and in the diatexitic gneiss at 680 mvd fit very well with the results in the suggested stress Domain 1. However, the results for both mafic gneiss (at 353 mvd) and veined gneiss (at 526 mvd) show significantly larger horizontal stress magnitudes.

5 INTERPRETATION OF PREVAILING STRESS FIELD AT OLKILUOTO

5.1 Introduction

Most of the employed stress measurement methods employed at the Olkiluoto site are relatively consistent with respect to magnitude levels of the principal stresses. However, they are regrettably inconsistent with respect to the orientation of the stresses. We have shown in this report that the overcoring data are consistent with one principal stress being vertical or near vertical and that this component is consistent with the theoretical weight of the overburden rock mass. These findings are verified by the production of axial fractures during hydraulic fracturing tests in near vertical drillholes (Klasson and Leijon, 1990, Ljunggren and Klasson, 1996) and normal stress values derived from hydraulic testing of pre-existing sub-horizontal fractures (Ask et al., 2010a). Hence, the primary remaining objectives are to resolve the orientation of the horizontal stress components and their orientation. In the following, the discussion is based on the general state of stress at the Olkiluoto site, i.e. it is assumed that all data are measuring the same continuum despite the fact that the investigated volume is relatively vast. As a result, the stress field locally may deviate from the interpretation made hereafter.

The hydraulic data and the data from tests with long strain gauges and LVDTs are consistent with respect to the orientation of σ_H; 92°, 80°, and 106°N. Only one convergence test contained useful information and suggested that σ_H is directed 156 °N. The acoustic emission data are regarded with skepticism as the internal errors in the derived solutions are much larger than all other methods. For this reason, these results are hereafter discarded. In Figure 5-1, the most reliable data are plotted as a function of vertical depth, also including some of the core discing results and the result of the re-evaluated overcoring data. Note that overcoring data correspond to the application of constraints 1+2, i.e. with one principal stress vertical and corresponding to density measurements on cores. In addition, by evaluating the resulting tangential stress, obviously incorrect data have been discarded (12 out of 25 tests discarded).

In Figure 5-1, it is clear that the various stress measuring methods do not indicate the very same stress field. The constrained overcoring data and the old hydraulic fracturing data the same trends for both σ_h and σ_H; σ_h being of the same order of magnitude as the vertical stress. These data suggest that the σ_H-magnitude is about 15 MPa around 300-400 mvd, but up to 45 MPa around 800 mvd. This implies that the σ_H-gradient must be strongly non-linear to avoid tensile values at surface. The recent hydraulic fracturing data is on the other hand relatively consistent with LSG+LVDT data; LSG+LVDT data indicate slightly larger magnitudes and some scatter in stress magnitudes. However, it should be pointed out that these data are not corrected for temperature and with a proper correction, these magnitudes will decrease to some extent. The convergence data point at about 280 m does not seem to be an outliers and the same is valid for several of the core discing solutions.

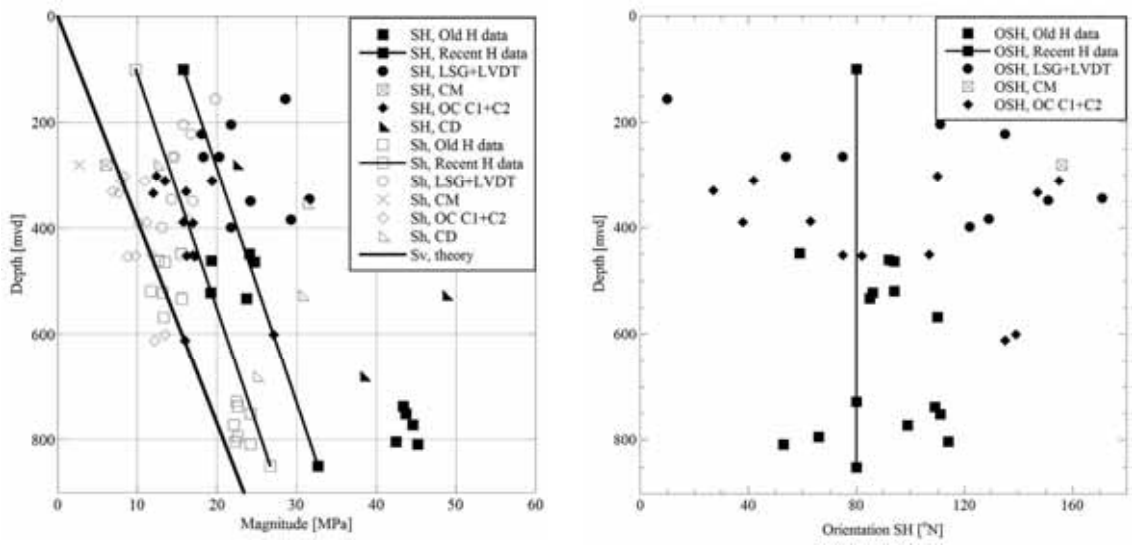

Figure 5-1. *All stress measurement results at the Olkiluoto site plotted as a function of vertical depth; stress magnitudes (left) and orientation of σ_H (right).*

When shifting focus to the orientation of σ_H, it is clear that it is not realistic to state that the observed scatter represent the true σ_H-orientation. What is especially surprising is that all methods display a considerable scatter. The old hydraulic fracturing data, which is generally a reliable methodology, indicate and orientation interval covering 50^o and 60^o at about 500 and 800 mvd, respectively. This is far from the repeatability observed when using hydraulic fracturing at other sites. Perhaps even more surprising is that the small scale overcoring and the large scale LSG+LVDT tests display similar and extreme scatter. Thus, a significant increase in scale has not improved repeatability. Conclusively, none of these data are useful for constraining the orientation of the stress field. The convergence test clearly did not generate conceivable stress magnitudes and this makes the determination of the orientation equally uncertain. This leaves only hydraulic data for estimation of stress orientation.

Rather than excluding data, the following suggested and most probable stress field will be based on hydraulic data, overcoring, core discing data, and LSG+LVDT data. Thus, the convergence data (and two out or four core discing solutions) are discarded. In the suggested stress profile (Figure 5-2), the σ_h-magnitude range is in the lower region controlled by the overcoring data and the upper limit by LSG+LVDT data. The σ_H-magnitude range is in the lower region controlled by overcoring data and by the σ_h-solution of the recent hydraulic data. The upper σ_H-magnitude range is controlled by previous hydraulic fracturing data and LSG+LVDT solutions. Note that when no emphasis is made to place weight on the various methods, the σ_h- and σ_H-intervals overlap (shaded area in Figure 5-2). For the σ_H-orientation, the suggested interpretation is based solely on hydraulic data.

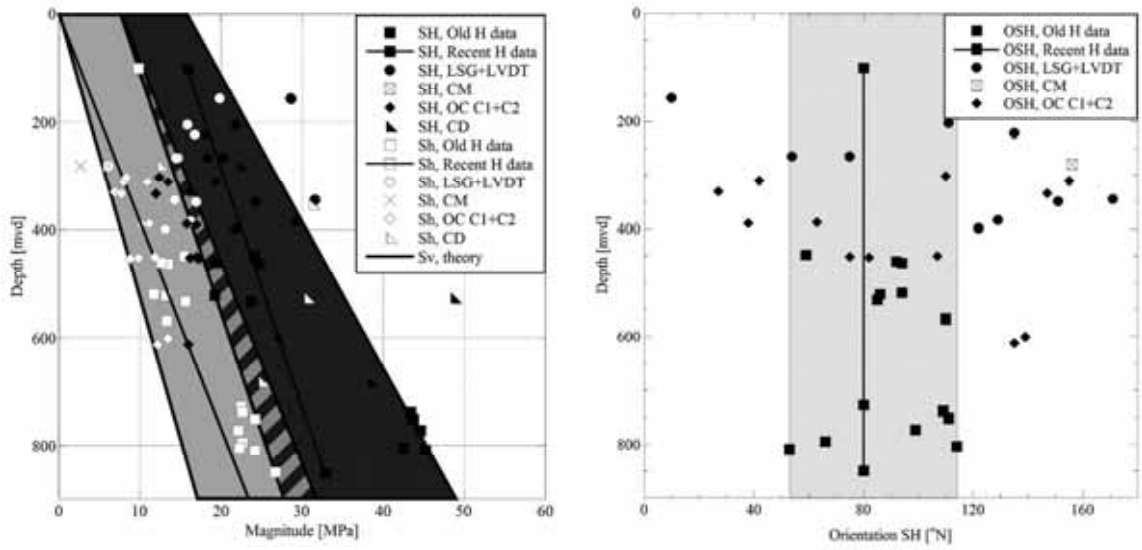

Figure 5-2. *General state of stress at the Olkiluoto site; stress magnitudes (left) and orientation of σ_H (right).*

REFERENCES

Aamodt RL, Kuriyagawa M, 1981. Measurements of instantaneous shut-in pressure in crystalline rock. *Proc. Workshop on Hydraulic Fracture Stress Measurements* (Eds. Zoback MD, Haimson BC), Monterey, USA. USGS, pp. 139-42.

Amadei B, Stephansson O, 1997. *Rock stress and its measurement*. Chapman & Hall, London, 490 pp.

Ask D, 2004. New developments of the integrated stress determination method and application to the Äspö Hard Rock Laboratory, Sweden. PhD thesis, Royal Institute of Technology (KTH), Stockholm.

Ask D, 2004. Evaluation of overcoring data in drillholes KFM01B, DBT-1, and DBT-3 and hydraulic stress data in drillhole KFM01A, KFM01B, KFM02A, and KFM04A at the Forsmark site. SKB report P-07-234, Svensk Kärnbränslehantering AB.

Ask D, Fontbonne F, Brunet C, 2010a. Hydraulic stress measurements in drillholes OL-KR40 and ONK-PP125 at the Olkiluoto site. Posiva Working Report (in press).

Ask D, Fontbonne F, Brunet C, 2010b. Complete stress field determination in an inclined boerhole at the Olkiluoto site, Finland: Joint inversion of hydraulic and en echelon data. *Proc. 5th Int. Symp. On In-situ Rock Stress*, August 25-27, 2010, Beijing, China.

Bredehoeft JD, Wolff RD, Keys WS, Schuter E, 1976. Hydraulic fracturing to determine the regional stress field, Piceance Basin, Colorado. *Bull.Geol. Soc. Am.*, 87, pp. 250-8.

Klasson H, Leijon B, 1990. Rock stress measurements in the deep drillholes at Kuhmo, Hyrynsalmi, Sievi, Eurajoki and Konginkangas. Report YJT-90-18. Nuclear Waste Commission of Finnish Power Companies, Helsinki.

Berg S, 2008. Overcoring rock stress measurements in drillhole ONK-PP169 & ONK-PP170. Posiva Working Report (in press).

Cornet FH, 1989. Material presented at the AGU meeting in 1989.

Cornet FH, 1993. The HTPF and the integrated stress determination method. In *Comprehensive Rock Engineering (JA Hudson Ed.), Vol 3*. Pergamon Press, Oxford, pp. 413-32.

Enever J, Chopra PN, 1989. Experience with hydraulic fracturing stress measurements in granites. *Proc. Int. Conf. On Rock Stress and Rock Stress Measurements* (Ed. Stephansson O), Stockholm. Centek Publisher, Luleå, pp. 411-20.

Fecker E, 2007. Rock stress measurements in ONKALO underground characterization facility at Olkiluoto at depth of 120 m. Posiva Work report 2007-26.

Gronseth JM, Kry PR, 1983. Instantaneous shut-in pressure and it's relationship to the minimum in-situ stress. *Proc. from the Hydraulic fracturing Stress Measurements*, Monterey, National Academy Press, Washington DC, pp. 55-60.

Haimson BC, Cornet FH, 2003. ISRM Suggested Methods for rock stress estimation – Part 3: hydraulic fracturing (HF) and/or hydraulic testing of pre-existing fractures (HTPF). *Int. J. Rock Mech. Min. Sci.*, 40, pp. 1011-20.

Hakala, M. 1999a. Numerical study on core damage and interpretation of in situ state of stress. Posiva report 99-25.

Hakala, M. 1999b. Numerical study of the core disk fracturing and interpretation of the in situ state of stress. *Proc. Ninth International Congress on Rock Mechanics (Paris, 1999)*, *2*, pp. 1149-1153. Rotterdam: A. A. Balkema.

Hakala M, 2000. Interpretation of the Hästholmen *in situ* state of stress based on core damage observations. Posiva report 2000-01.

Hakala M, 2004. Personal communication.

Hakala, M. 2008. Shaft response and shaft strain measurements at Olkiluoto. Posiva Working Report (in preparation).

Hakala, M. 2010a. LSG report

Hakala, M. 2010b. LVD report

Hast N, 1958. The state of stress in the upper part of the earth's crust. *Eng. Geol.*, 2, pp. 5-17.

Hayashi K, Haimson BC, 1991. Characteristics of shut-in curves in hydraulic fracturing stress measurements and determination of in-situ minimum compressive stress. *J. Geophys. Res.*, 96, pp. 18311-21.

Ito T, Evans K, Kawai K, Hayashi K, 1999. Hydraulic fracturing reopening pressure and the estimation of maximum horizontal stress. *Int. J. Rock Mech. Min. Sci. & Geomech. Abstr.*, 36, pp. 811-26.

Lee MY, Haimson BC, 1989. Statistical evaluation of hydraulic fracturing stress measurement parameters. *Int. J. Rock Mech. Min. Sci. & Geomech. Abstr.*, 26, pp. 447-56.

Lehtonen A, 2005. Evaluation of rock stress estimation by the Kaiser effect. Posiva Working report 2005-67.

Lehtonen, A. 2008. Kaiser Effect-based stress measurements in Olkiluoto drillholes KR28 and KR29. Posiva Working Report (in press).

Lindfors, U., Perman, F., Sjöberg, J. 2004. Evaluation of the overcoring results from drillhole KFM01B. SKB. P-report P-05-66.

Ljunggren C, Klasson H, 1996. Rock stress measurements at the three investigations sites, Kivetty, Romuvaara, and Olkiluoto, Finland. Volumes 1 and 2. Posiva Work report PATU-96-26e.

Andersson, J., Ahokas, H., Hudson, J.A., Koskinen, L., Luukonen, A., Löfman, J., Keto, V., Pitkänen, P., Mattila, J., Ikonen, A.T.K., Ylä-Mella, M. Olkiluoto Site Description 2006. Posiva report 2007-03.

Parker RL, McNutt MK, 1980. Statistics for one-norm misfit measure. *J. Geophys. Res.*, 85, pp. 4429-30.

Ratigan JL, 1992. The use of the fracture reopening pressure in hydraulic fracturing stress measurements. *Rock Mech. Rock Eng.*, 25, p. 125-136.

Rutqvist J, Tsang C-F, Stephansson O, 2000. Uncertainty in the principal stress estimated from hydraulic fracturing measurements due to the presence of the induced fracture. *Int. J. Rock Mech. Min. Sci. & Geomech. Abstr.*, 37, pp. 107-20.

Sjöberg J, 2003. Overcoring rock stress measurements in drillhole KR24, Olkiluoto. Helsinki, Finland. Posiva Work report 2003-60.

Suomen Malmi Oy, 2006. Jännitystilamittaus Olkiluodossa V. 2005-2006. Rapportti 225/2605/06/JM, RN.

Sjöberg J, Christiansson R, Hudson JA, 2003. ISRM Suggested Method for Rock Stress Estimation: Part 2 — Overcoring Methods. *Int. J. Rock Mech. Min. Sci.*, *40*, No. 7-8, pp. 999-1010.

APPENDIX 1: CORE DISCING DATA

Table A1-1. *Core discing data at Olkiluoto.*

				Shape										Width	
Drillhole	Start [m]	End [m]	Rock type	(([pcs]	(| [pcs]	| ([pcs]	)) [pcs]	) | [pcs]	|) [pcs]	| | [pcs]	) ([pcs]	S [pcs]	A [pcs]	Min [mm]	Max [mm]
OL-KR1	484.52	484.55	PGR				1			1			1	6	7
OL-KR1	784.54	784.55	VGN							1		1	1	4	10
OL-KR1	877.06	877.16	VGN							2			5	5	
OL-KR1	945.36	945.40	TGG										3		
OL-KR1	968.32	969.87	PGR				2	1	1	4		5	20	15	30
OL-KR2	607.68	607.71	PGR	1						1					
OL-KR2	736.75	736.86	DGN									3	10	37	
OL-KR2	737.73	737.51	DGN										X		
OL-KR2	862.08	862.12	PGR										4		
OL-KR2	889.90	889.97	PGR							1		2	1	33	42
OL-KR2	944.68	944.74	TGG				2						6		
OL-KR2	1019.72	1019.74	DGN										2		
OL-KR4	592.31	592.32	PGR				2			1					
OL-KR4	816.34	816.61	PGR	1					2				X	4	25
OL-KR4	818.16	818.19	PGR	2										33	
OL-KR4	821.48	823.26	PGR										X		
OL-KR4	842.15	842.30	PGR										X		
OL-KR4	848.10	850.10	PGR				1			4				16	29
OL-KR4	853.80	853.95	PGR										X		
OL-KR5	328.18	328.32	PGR										X		
OL-KR7	542.32	542.33	PGR					1	1					11	
OL-KR7	711.77	711.80	PGR		1			1		1				15	12

Table A1-1. *Core discing data at Olkiluoto (continued).*

				Shape										Width	
Drillhole	Start [m]	End [m]	Rock type	(([pcs]	(| [pcs]	| ([pcs]	)) [pcs]	) | [pcs]	|) [pcs]	| | [pcs]	) ([pcs]	S [pcs]	A [pcs]	Min [mm]	Max [mm]
OL-KR8B	595.87	596.36	PGR	1			2			5	3			5	41
OL-KR10	599.82	599.83	VGN										2	12	
OL-KR10	600.89	600.90	VGN	1						1				3	
OL-KR11	314.69	314.79	PGR										5	15	30
OL-KR11	600.96	601.18	VGN	5		1					1		18	2	30
OL-KR11	768.28	768.29	VGN				1						1	5	5
OL-KR11	946.87	946.92	MGN					1					13	1	10
OL-KR11	973.19	973.22	PGR				1						3	6	13
OL-KR12	523.48	523.50	VGN							2				17	
OL-KR12	622.50		MGN							1					
OL-KR12	633.84		DGN	1											
OL-KR12	760.03		VGN				1								
OL-KR16	154.95	155.19	VGN				1								
OL-KR16B	29.06	30.63	DGN											100	
OL-KR16B	34.56	37.45	MGN											10	>100
OL-KR16B	37.45	38.27	PGR											10	>100
OL-KR19	368.90	368.92	MFGN									1	1	20	
OL-KR19	487.14	487.41	PGR	1						1					
OL-KR23	407.17	411.52	MGN/VGN												
OL-KR23	415.46	420.26	PGR/VGN	3						1		5			
OL-KR23	446.64	447.64	VGN	2								1			
OL-KR23	450.15		PGR	1											

Table A1-1. *Core discing data at Olkiluoto (continued).*

				Shape										Width	
Drillhole	Start [m]	End [m]	Rock type	(([pcs]	(| [pcs]	| ([pcs]	)) [pcs]	) | [pcs]	|) [pcs]	| | [pcs]	) ([pcs]	S [pcs]	A [pcs]	Min [mm]	Max [mm]
OL-KR24	310.61	310.70	VGN												
OL-KR24	314.48		VGN												
OL-KR24	384.17	387.10	MGN												
OL-KR27	388.46	388.48	PGR									1	4		
OL-KR43	985.35	985.56	PGR												
				19	**1**	**1**	**14**	**4**	**4**	**27**	**4**	**19**	**>100**		